Volume 9 | Number 12 | December 2016 | Pages 3561–3796

Energy & Environmental Science

www.rsc.org/ees

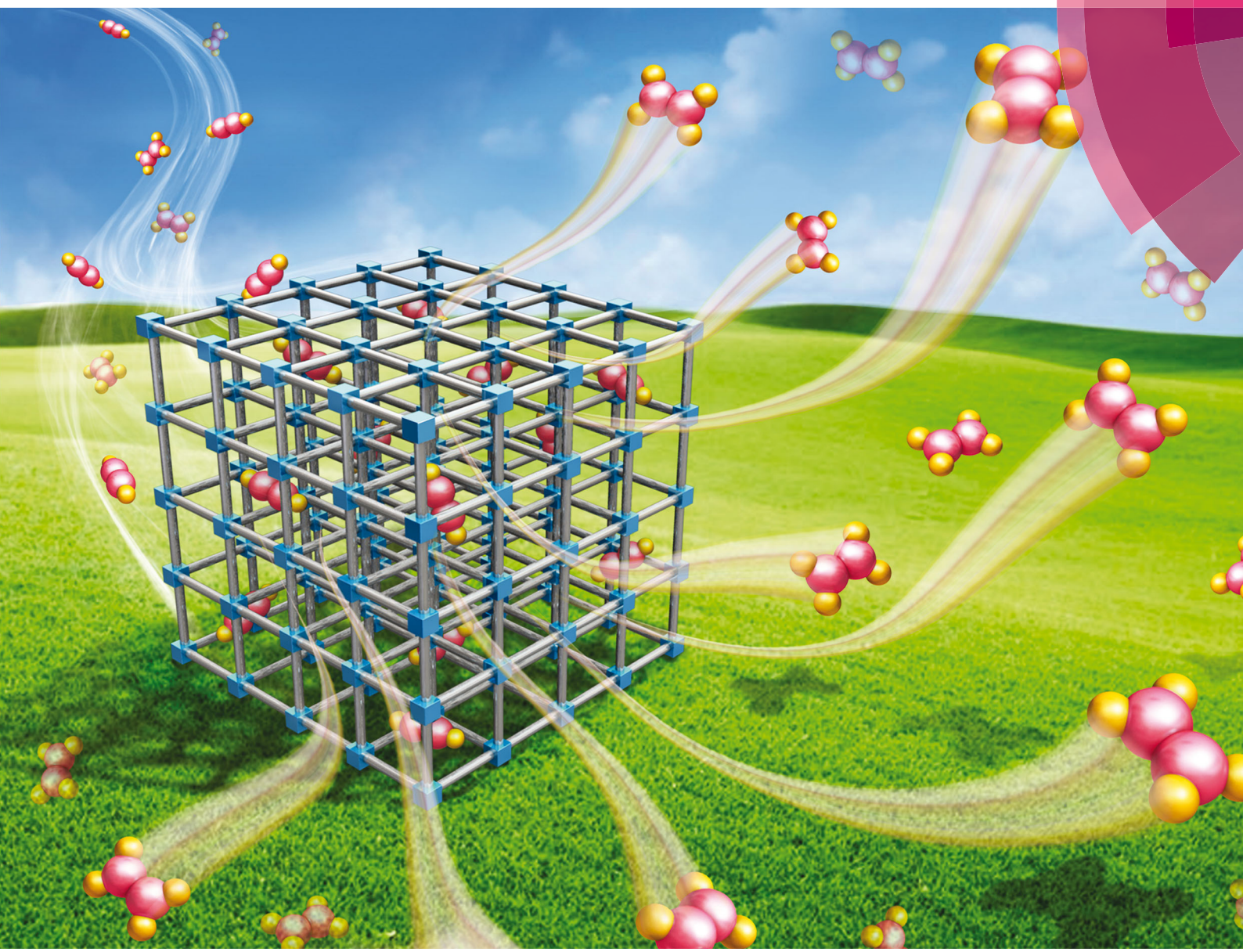

ISSN 1754-5692

ROYAL SOCIETY OF CHEMISTRY

REVIEW ARTICLE
Banglin Chen *et al.*
Potential of microporous metal–organic frameworks for separation of hydrocarbon mixtures

175 YEARS

Energy & Environmental Science

REVIEW

View Article Online
View Journal | View Issue

Cite this: *Energy Environ. Sci.*, 2016, **9**, 3612

Potential of microporous metal–organic frameworks for separation of hydrocarbon mixtures

Zongbi Bao,[ab] Ganggang Chang,[ab] Huabin Xing,[a] Rajamani Krishna,[c] Qilong Ren[a] and Banglin Chen*[b]

Received 30th June 2016,
Accepted 30th August 2016

DOI: 10.1039/c6ee01886f

www.rsc.org/ees

In the process industries, the separation of mixtures of hydrocarbons is important both for the preparation of feedstocks and for use as end products. The constituents, hydrocarbons, are either aliphatic or aromatic, saturated or unsaturated, with a large variation in the number of carbon atoms. Using microporous metal–organic frameworks (MOFs), a number of different separation strategies can be employed to achieve the desired separation performance. The strategies include selective binding with the metal atoms of the framework, exploiting differences in molecular packing efficiencies within the ordered pore structures, utilizing selectivities based on the framework flexibility and gate-opening mechanisms, and molecular sieving. Various strategies are discussed in this article, along with perspectives for future research and development for improving the separation performance.

Broader context

While CO_2 capture in pre- and post-combustion processing garners a lot of current research interest in the development of novel materials such as metal–organic frameworks (MOFs), there is a much wider scope for utilizing MOFs for separation of hydrocarbon mixtures. The main purpose of this article is to highlight the wide variety of separation strategies that are employable in this task. Particularly noteworthy is the exploitation of the differences in the stacking of aromatic molecules within ordered crystalline MOF structures. Just to give one example, unlike traditionally used zeolitic materials, MOFs can be synthesized to yield one-dimensional triangular-shaped channels; this geometry offers unique separation possibilities that are not possible with other materials.

1. Introduction

The separation of hydrocarbon mixtures represents one of the most important chemical processes in the petrochemical industry. Hydrocarbons that are exclusively composed of carbon and hydrogen atoms can be categorized into alkanes or paraffins, alkenes or olefins, and aromatic hydrocarbons based on their chemical nature. Among the hydrocarbons, olefins (ethylene, propylene and butadiene) and aromatic hydrocarbons (benzene, toluene and the isomers of xylene) are important feedstocks that are further converted into more useable consumer and industrial products. Hydrocarbon separations involving light hydrocarbons (C1–C4), isomers of alkanes, and C8-aromatics (*ortho*-xylene (OX), *meta*-xylene (MX), *para*-xylene (PX), and ethyl benzene (EB)) are of industrial importance. Typically, alkane/alkene separations are achieved by cryogenic distillation, an energy-intensive and capital-intensive process.[1] A large number of distillation stages and a high reflux ratio are required in order to achieve sometimes a polymer-grade monomer, and the process must be operated at cryogenic temperatures and high pressures. It is desirable to develop alternative technologies that might enable this process to be carried out with lower energy costs.

Separation by means of adsorption using porous materials is recognized as a promising alternative where the gases are adsorbed into the pores of the material and desorbed as a function of temperature or pressure. Although inorganic and carbon-based materials have been successfully applied for such commercial applications since the mid-1990s, improvements in separation efficiency provide a strong motivation for studying the behavior of hydrocarbon molecules within newly reported porous materials. The past three decades have witnessed an explosive growth in research and development of crystalline

[a] *Key Laboratory of Biomass Chemical Engineering of Ministry of Education, College of Chemical and Biological Engineering, Zhejiang University, Hangzhou 310027, P. R. China*
[b] *Department of Chemistry, University of Texas at San Antonio, One UTSA Circle, San Antonio, Texas 78249-0698, USA. E-mail: banglin.chen@utsa.edu; Fax: +1-210-458-7428*
[c] *Van't Hoff Institute for Molecular Sciences, University of Amsterdam, Science Park 904, 1098 XH Amsterdam, The Netherlands*

nanoporous materials. Particularly, the discovery of a new class of synthetic porous materials, metal–organic frameworks (MOFs),[2–5] also called porous coordination polymers (PCPs),[6,7] or porous coordination networks (PCNs),[8,9] has received considerable attention in the past two decades as they offer great opportunities for revolutionizing industrial applications, especially in the storage, separation and purification of gases.[10–18] Compared to traditional porous materials, MOFs possess numerous interesting and appealing features, including a large internal surface area and pore volume, perfectly ordered and well-defined pore structures, functionalized pore surfaces, and adjustable pore dimensions. Besides, in some cases structural flexibility sensitivity to external stimuli enables MOFs to have specific properties such as pressure/temperature dependent molecular sieving, therefore showing outstanding separation performances, which may be difficult to attain with a rigid porous material such as a zeolite or activated carbons. Moreover, the boundless chemical tunability of the pore geometry and surface functionality within MOFs can facilitate control over adsorption selectivity, and high surface areas/pore volume generally give rise to a large separation working capacity.

Generally speaking, the adsorption separation of hydrocarbons in MOFs, as observed for other gaseous separations in MOFs, can be achieved *via* equilibrium, steric, kinetic or gate-opening mechanisms or combinations thereof. For equilibrium separation, the pore aperture of the adsorbent should be large enough to allow all adsorbates to pass, and the separation performance depends on the differences between the relative affinities of various adsorbates and the adsorbent surface. The interaction strength is decided by the surface characteristics of the adsorbent and the properties of the targeted adsorbate molecule, and it is usually characterized by the magnitude of the isosteric heat of adsorption. Separation based on a steric mechanism is a consequence of shape/size exclusion or the molecular sieving effect, when some adsorbate species cannot get through the pore openings while others can. Kinetic separation, also known as partial molecular sieve action, is achieved by virtue of the differences in diffusivities of guest molecules. Guest molecules with substantially higher mobilities will occupy the pore spaces more quickly than tardier guest molecules; such differences in diffusivities can be exploited in transient fixed bed separations. The gate-opening-based process is associated with structural transition from a closed non-microporous phase to an open porous phase induced by gas sorption in which specific threshold pressures control the uptake and release of individual molecules. These mechanisms have been elucidated in several monographs and review articles.[17,19–23] In this feature article, we will highlight some important advances in the development of porous metal–organic frameworks for the separation of industrially important hydrocarbons.

2. Metal–organic frameworks for light hydrocarbon separation

The separation of light hydrocarbons including methane, acetylene, ethylene, ethane, propane, and propylene is a very important industrial process because these light hydrocarbons have been widely utilized as energy sources and raw materials in the petrochemical industries. For example, methane, the primary component of natural gas, is a cleaner alternative to other automobile fuels such as gasoline and diesel; ethane is the principal feedstock for the production of ethylene by means of steam cracking. Both acetylene and ethylene are the very basic raw materials for various industrial and consumer products such as acetic acid, rubber and plastics. Efficient utilization of these light hydrocarbons generally requires high quality and purity.

2.1 Adsorptive separation of methane over C2 hydrocarbons

The separation of methane from acetylene is one of the most important processes in the field of gas purification. Acetylene is principally obtained from the cracking of natural gas.[24] The separation of acetylene from methane is necessary to meet the requirements of Grade A (no more than 0.5% impurities) acetylene for the organic synthesis. Additionally, some ongoing chemical processes for oxidative coupling of methane to C2 hydrocarbons (C_2H_x, x = 2, 4, 6) ultimately need to separate methane from C2 hydrocarbons because of incomplete methane conversion.[25–27] Given the large differences in the physical properties between methane and C2 hydrocarbons, both size selective effects and framework–hydrocarbon interactions can be utilized to achieve a high selectivity within a metal–organic framework. There have been a large number of reports regarding C2 hydrocarbon/methane separations on metal–organic frameworks with significantly high selectivities.[28–57]

Considering the fact that the very important role of open copper metal sites to direct their bonding with acetylene molecules, as exemplified in **Cu_3(btc)$_2$** (btc = benzene-1,3,5-tricarboxylic acid) and **MOF-505**, we synthesized a microporous MOF **Cu_2(ebtc)** (ebtc = 1,1′-acetylenebenzene-3,3′,5,5′-tetracarboxylate) by incorporating a triple C≡C bond into the BPTC (3,3′,5,5′-biphenyltetracarboxylate) organic linkers. This framework is a **MOF-505** analogue of NbO topology with a high surface area and open Cu^{2+} sites, and an extraordinarily high (252 $cm^3\ g^{-1}$) acetylene uptake capacity – nearly 10 times higher than that of methane at 293 K. The adsorption strength towards acetylene in this material is significantly higher than in **Cu_3(btc)$_2$** and **MOF-505**. This enforced interaction might be attributed to the additional weak interactions between the triple C≡C bond of acetylene and the organic linker.[58]

Microporous MOFs with the pore size comparable to the kinetic diameters of small hydrocarbons may be highly selective for the separation of small hydrocarbons because of a strong confinement effect in the micropores. For example, Chen *et al.* reported a two-dimensional microporous metal–organic framework **Cu(bdc-OH)** with functional OH groups on the pore surfaces for the selective adsorption of C_2H_2/CH_4 at room temperature. This framework has 1D channels of a size of about 3.0 Å and exhibits a C_2H_2/CH_4 selectivity of 6.7 at 296 K.[59] By means of framework interpenetration they also have targeted some microporous MOFs with pore sizes of 3.1 to 4.8 Å for the selective adsorptive separation of C_2H_2, C_2H_4, and C_2H_6 from CH_4. For example, the small pores tuned by the double framework

interpenetration have enabled **UTSA-38a** as the selective porous material for the separation of CO_2/CH_4, C_2H_2/CH_4, C_2H_4/CH_4, and C_2H_6/CH_4 with a calculated Henry's law separation selectivity of 3.3, 5.6, 6.4, and 10.1, respectively.[60] A doubly interpenetrated cubic metal–organic framework **UTSA-36a** $[Zn_2(pba)_2(bdc)]$ (Hpba = 4-(4-pyridyl)benzoic acid, H_2bdc = 1,4-benzenedicarboxylic acid) was reported to exhibit highly selective gas sorption of C_2H_6, C_2H_4 and C_2H_2 over CH_4 with Henry's law selectivities of 11 to 25 in the temperature range of 273 to 296 K.[52] A triply interpenetrated mixed metal–organic framework $Zn_2(bba)_2(CuPyen)$ (**M′MOF-20**; bba = biphenyl-4,4′-dicarboxylate) with the pore size of 3.9 Å shows a C_2H_2/CH_4 selectivity of 34.9,[41] and the four-fold interpenetrated framework $Zn_5(bta)_6(tda)_2$ (bta– = 1,2,3-benzenetriazolate, tda– = thiophene-2,5-dicarboxylate) displays an IAST (ideal adsorbed solution theory) selectivity of 15.5 for an equimolar acetylene/methane mixture at 295 K, but an acetylene uptake capacity of only 1.96 mmol g^{-1} at 1 bar.[61] However, these materials suffer from acetylene capacity limitations because of low BET surface areas (<700 m^2 g^{-1}).

To rationalize the structure–property relationship and thus to maximize the C2/C1 separation selectivity and capacity, we proposed two microporous metal–organic frameworks **UTSA-33** $[Zn_4L]$ and **UTSA-34** $[Cu_3(H_2L)]$ derived from a novel octacarboxylate linker (H_8L = 1,2,4,5-tetra(5-isophthalate)benzene). The former, endowed with small pores of about 4.8 to 6.5 Å, shows highly selective separation of C2 hydrocarbons from methane with adsorption selectivities of 12 to 20 at room temperature as well as a moderate acetylene capacity of 97.1 mg g^{-1} at 1 atm,[42] while the latter has cage sizes of about 12.8 Å and exhibits the highest separation capacity of 3.0 mol kg^{-1} and selectivity of 35 among the materials ever reported for the separation of C2 hydrocarbons from methane at room temperature.[54] Their separation performance of C2 hydrocarbons from methane has been further established by simulated breakthrough using an equimolar four-component mixture of C_2H_2, C_2H_4, C_2H_6 and CH_4 in **UTSA-33** and **UTSA-34** along with the well-examined **ZIF-8**. It was expected that the breakthrough of all C2s was retained significantly later with **UTSA-34** as a result of the high pore volume and/or immobilized open copper sites within the framework. In addition, **UTSA-34** also exhibits a much higher capacity and separation selectivity in the equimolar binary mixture of C_2H_6 and CH_4 than **ZIF-8**.[54]

The separation of C_2H_6 from CH_4 has also been investigated by Kitagawa *et al.*[62] in the flexible two-dimensional frameworks, **CID-5** [Zn(5NO_2-ip)(bpy) (ip = isophthalate, bpy = 4,4′-bipyridine)] and CID-6 [Zn(5MeO-ip)(bpy)], and their solid solutions **CID-5/6** $[Zn(5NO_2\text{-ip})_{1-x}(5MeO\text{-ip})_x(bpy)$ (x = 0.1, 0.2, 0.4)]. **CID-5** and **CID-6** exhibit distinct framework flexibility that may be caused by the size/shape and electron-donating/-withdrawing properties of the substituent group of the ligands and the resulting packed structures. The structure flexibility of **CID-5** is larger than that of **CID-6**. The porosity and flexibility of **CID-5/6** depend on the relative ratio of the ligands in the framework. **CID-5/6** (x = 0.1) has a crystal structure similar to that of the pure **CID-5**, whereas **CID-5/6** (x = 0.2, 0.4) is more closely related to the pure **CID-6**. **CID-5** and **CID-5/6** (x = 0.1) show a kind of gate-opening behavior towards C_2H_6 adsorption. It was found that different framework flexibilities could lead to different kinetic breakthrough curves for a binary CH_4–C_2H_6 gas mixture. The two pure CID frameworks did not demonstrate appropriate separation properties while **CID-5/6** (x = 0.1) can selectively adsorb C_2H_6 from CH_4. Thus, the gas separation efficiencies can be optimized by precise tuning of the flexibility in the ligand-based solution compounds.[62] The same group investigated the separation of C2 hydrocarbons (C_2H_4 and C_2H_6) from CH_4 mixtures on a lanthanum-based framework La(btb) (H_3btb = 1,3,5-tris(4-carboxyphenyl) benzene)), which showed unprecedented water and chemical stability. This framework possesses 1D hexagonal channels decorated with open La sites and the aperture size is *ca.* 10 Å. At 273 K and pressure up to 10 atm, the IAST-predicted selectivities for C_2H_6/CH_4 and C_2H_4/CH_4 remain larger than 8, which even outperformed that for CO_2/CH_4. Interestingly, La(btb) prefers to capture the C2 hydrocarbons rather than CO_2 probably because of weaker electrostatic interactions between C_2H_6 molecules than that of CO_2. The breakthrough experiments showed that La(btb) could provide complete separation of C_2H_6 from CH_4. The *in situ* DRIFT spectra study revealed that the open coordination site of the exposed La^{3+} cations may account for such excellent separation performance.[63]

Adsorptive separation of small hydrocarbons could also be realized based on the temperature-induced molecular-gating effects in a MOF-based mesh-adjustable molecular sieve. Zhou and co-workers[64] reported for the first time a mesh-adjustable MOF $Ni_8(5\text{-bbdc})_6(\mu_3\text{-OH})_4$ (**MAMS-1**; 5-bbdc = 5-*tert*-butyl-1,3-benzenedicarboxylate). This material consisted of interconnected hydrophilic channels and hydrophobic chambers. Gas molecules enter the hydrophobic gas-storage chambers through the hydrophilic channels and gates in the hydrophobic/hydrophilic interface. Interestingly, the gates of **MAMS-1** could open linearly as the temperature increases, thus the size of the gates can be tuned continuously from 2.9 to 5.0 Å. This means any two gases with a size difference can in principle be separated by precise temperature control. The smaller molecules could preferentially enter into the hydrophobic chambers, corresponding to higher uptake. For example, **MAMS-1** can selectively adsorb methane from ethylene at 143 K, ethylene from propylene at 195 K, and propylene from isobutane at 241 K.[64] In the follow-up study by the same group, three isostructural mesh-adjustable molecular sieves, **MAMS-2**, **MAMS-3**, and **MAMS-4**, were further explored for gas separation. These new MAMSs all display a temperature-induced molecular sieving effect similar to that observed in **MAMS-1**, although they are isostructural but quite different from the structure of **MAMS-1**. As temperature increases, the gates of the new MAMSs can be finely tuned in the range of 2.9–4.6 Å. Similar to **MAMS-1**, **MAMS-2** can also distinguish methane from ethylene at 143 K, ethylene from propylene at 195 K, and propylene from isobutane at 231 K.[65]

Herein it is very necessary to highlight the remarkable performance of C1 and C2 hydrocarbon separations on a serial of isostructural **MMOF-74** (M = Fe, Mg, Co) because of their high surface area and high density of open metal sites. Long and co-workers recently demonstrated the extraordinary prospects

for using the metal–organic framework **FeMOF-74** as a solid adsorbent in the separation of a mixture of methane, ethane, ethylene, and acetylene to obtain each individual component in a nearly pure form.[66] In addition to **FeMOF-74**, both **MgMOF-74** and **CoMOF-74** also perform well in the separation of methane from an equimolar $CH_4/C_2H_2/C_2H_4/C_2H_6$ mixture at 296 K and 1 bar of total pressure.[67] Plonka and co-workers recently reported the adsorption of methane, ethane, ethylene and acetylene in two microporous calcium-based MOFs with 1D open channels.[68] Both materials are highly selective toward C2 hydrocarbon gases over methane with a maximum C2/C1 selectivity of 74 for ethane/methane. The breakthrough simulation data confirmed that both materials can separate methane from C2 hydrocarbons.

Considering the importance of chlorofluorocarbons (CFCs) in many applications including fluoropolymers, refrigerants, propellants and so forth, it is worth introducing Thallapally's recent work on the adsorption of small CFCs in the MOF materials.[69] Four CFCs including dichlorodifluoromethane (R12), chlorodifluoromethane (R22), chlorotrifluoromethane (R13), tetrafluoromethane (R14) and difluoromethane (R32) were used to explore the possibility of separating these azeotropic mixtures of fluorocarbons on **MMOF-74** (M = Ni, Co), **MIL-101(Cr)** and **MIL-100(Fe)**. Among these MOFs, **MIL-101** was found to show an exceptionally high uptake capacity reaching >14 mmol g^{-1} at a relative pressure of 0.4 and ambient temperature because of its high porosity and high density of open Cr metal sites. The difference in both adsorption strength and uptake for CFCs could be related to their polarizability and molecular volume. Both simulation and experimental breakthrough measurements confirmed that **MIL-101** could effectively separate the CFC mixture into individual fractions.

2.2 Adsorptive separation of acetylene over ethylene

Ethylene and acetylene are widely used as chemical feedstocks in the manufacture of many polymer products, in most of which the high purity of starting materials is a prerequisite. Acetylene is one of the major byproduct in the process of steam cracking of ethane to produce ethylene. It is also an impurity of approximately 1% concentration produced in a naphtha cracker during ethylene production. There are strict limitations to the amount of acetylene that can be tolerated in the feed to an ethylene polymerization reactor because the presence of acetylene at levels higher than 40 ppm will poison the catalyst. Therefore, the recovery or removal of acetylene from ethylene streams is essential. Acetylene/ethylene separation is a very important but challenging industrial separation task because of their similar molecular sizes, volatilities and electronic structures based on unsaturated C–C bonds. The selective removal of acetylene is conventionally carried out by an energy-intensive absorption process using liquid *N*,*N*′-dimethylformamide, but the use of solid adsorbents could potentially provide an energy efficient alternative. In reality, the separation performance of the acetylene/ethylene mixture has been extensively examined in metal–organic frameworks, but only a few of them show some promise.[35,44,45,56,66,70–73]

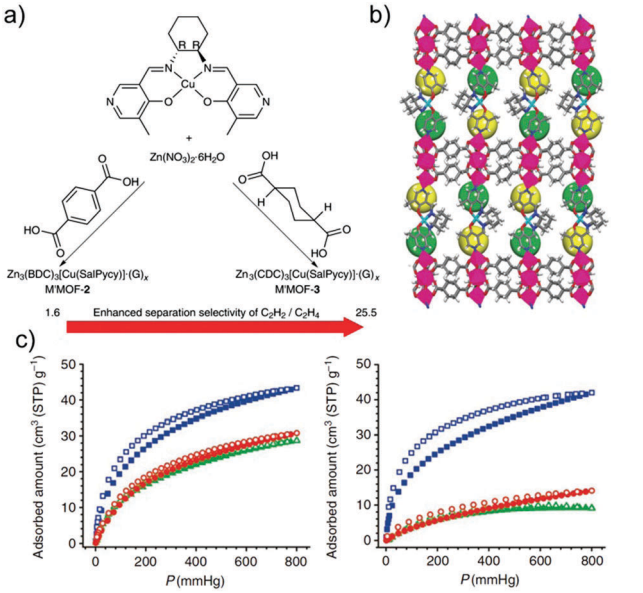

Fig. 1 (a) Syntheses and structures of **M′MOFs-2** and **-3**. (b) The three-dimensional (3D) pillared framework with chiral pore cavities for **M′MOF-3**. (c) Adsorption isotherms of C_2H_2 (blue square), CO_2 (red dot) and C_2H_4 (green triangle) on **M′MOF-2a** (left) and **M′MOF-3a** (right) at 295 K.[70]

Xiang *et al.* reported the first example of microporous metal–organic frameworks capable of fulfilling this challenging separation.[70] Two mixed-metal–organic frameworks (M′MOFs), $Zn_3(BDC)_3[Cu(SalPycy)]$ (**M′MOF-2**) and $Zn_3(CDC)_3[Cu(SalPycy)]$ (**M′MOF-3**) (Fig. 1), were readily assembled by solvothermal reactions between pre-constructed chiral metalloligand Cu(SalPyCy) and $Zn(NO_3)_2{\cdot}6H_2O$ and H_2BDC (BDC = 1,4-benzenedicarboxylate) or H_2CDC (CDC = 1,4-cyclohexanedicarboxylate), respectively. **M′MOF-2** and **M′MOF-3** are isostructural three-dimensional frameworks, in which $Zn_3(COO)_6$ secondary building blocks are bridged by BDC or CDC anions to form two-dimensional tessellated $Zn_3(BDC)_3$ or $Zn_3(CDC)_3$ sheets that are further pillared by the chiral metalloligand Cu(SalPyCy). Adsorption isotherms of CO_2 at 195 K on these two activated M′MOFs (denoted as **M′MOF-2a** and **M′MOF-3a**), with hysteric sorption characteristics, indicate that they both feature framework flexibility. At 195 K **M′MOF-2a** can adsorb both C_2H_2 and C_2H_4 to give a low Henry's law selectivity of 1.6; however, **M′MOF-3a** displays a significantly higher C_2H_2/C_2H_4 selectivity of 25.5 because of the smaller pore aperture within **M′MOF-3a**. The more flexible CDC in **M′MOF-3a** has enabled the framework **M′MOF-3a** less rigid than **M′MOF-2a**, thus resulting in narrower pores in **M′MOF-3a**. The narrower molecular size of C_2H_2 ($3.32 \times 3.34 \times 5.70$ Å) compared with that of C_2H_4 ($3.28 \times 4.18 \times 4.84$ Å) has enabled the full entrance into the micropores in **M′MOF-3a**, but C_2H_4 molecules are basically blocked or the kinetics are very slow. Remarkably, a C_2H_2/C_2H_4 separation selectivity of 5.2 at 295 K makes **M′MOF-3a** a practically promising adsorbent for this important separation.[70]

Such an approach for constructing M′MOFs is very appealing to design some functional porous materials that are able to maximize their size-selective effects. In the follow-up work,

they further devised four isostructural mixed-metal–organic frameworks (**M′MOFs-4–7**) in which the pore space and framework flexibility could be systematically tuned by the interplay of both the metalloligands and organic ligands.[74] Changing the metalloligand from Cu(SalPyMeCam) to Cu(SalPytBuCy) systematically reduces the accessible pore space. These activated M′MOFs are promising for the selective separation of ethylene and acetylene at room temperature. The acetylene uptakes for these M′MOFs are systematically higher than ethylene uptakes under ambient conditions, giving the IAST selectivities based on a 1/99 C_2H_2–C_2H_4 gas mixture at 296 K and a total pressure of 100 kPa ranging from 5 to 15. Among these MOFs, **M′MOF-4a** scores high on both C_2H_2/C_2H_4 adsorption selectivity and C_2H_2 uptake. The potential application of these M′MOFs for the fixed bed adsorption separation of C_2H_2/C_2H_4 has been further examined and compared by transient breakthrough simulations with a step input of a 1/99 C_2H_2–C_2H_4 mixture at 296 K and total pressures of 100 kPa. The separation performance decreases in the order of **M′MOF-4a** > **M′MOF-6a** > **M′MOF-5a** > **M′MOF-7a**. In order to satisfy the feedstock requirements for the polymerization reactor, an acetylene content less than 40 ppm in the outlet gas can be readily fulfilled by the fixed bed **M′MOF-4a** adsorber.

Along with the aforementioned mixed metal–organic frameworks, He *et al.*[67] examined the potential of other MOFs with open metal sites (*e.g.* **MgMOF-74**, **CoMOF-74**, **Cu_3(btc)$_2$**, **PCN-16**, **NOTT-101/102**, **UTSA-20**, **MOF-505**, and **UMCM-150**) for ethylene/acetylene separations by performing transient breakthrough calculations. Considering the fact that ethylene produced in a naphtha cracker contains an impurity of approximately 1% acetylene, a binary C_2H_2/C_2H_4 mixture containing 10 000 ppm of C_2H_2 was used as the model feed gas. It was found that the IAST selectivity of C_2H_2/C_2H_4 adsorption *versus* the volumetric uptake capacity of C_2H_2 is best performed on **M′MOF-3a**, whereas the higher capacity for C_2H_2 uptake is found on **MgMOF-74** and **CoMOF-74**. Indeed, the separation characteristics of the PSA unit are dictated by a combination of adsorption selectivity and uptake capacity. In terms of breakthrough time at a given C_2H_2 concentration of 40 ppm in the outlet gas, the hierarchy of production capacities decreases in the order of **MgMOF-74** > **CoMOF-74** > **M′MOF-3a** > **M′MOF-4a**. The superior performance of **MgMOF-74** and **CoMOF-74** can be traced to their high capacities to adsorb C_2H_2. **M′MOF-3a** and **M′MOF-4a** have high selectivities but are subject to capacity limitations.[67] Similarly, Long and co-workers reported that **FeMOF-74** performs even better for this challenging separation owing to the softer nature of open Fe^{2+} metal sites as well as its ability for π-back-bonding compared to Mg^{2+} and Co^{2+} ions.[66]

It is worth mentioning that He *et al.* reported the first example of microporous hydrogen-bonded organic frameworks (HOFs) with permanent porosity and the capacity for extraordinarily highly selective separation of C_2H_2 and C_2H_4 at ambient temperature.[75] **HOF-1** is a three-dimensional porous HOF in which each organic building block is connected with four neighboring ones by eight strong hydrogen bonds involving 2,4-diaminotriazine groups. One of the amine groups within the 2,4-diaminotriazine moieties is not involved in the hydrogen bonding and thus is exposed on the pore surfaces for potential interactions with gas molecules. The C_2H_2/C_2H_4 molar ratio separation selectivity of 7.6 in **HOF-1a** is significantly higher than those previously reported (<2.5) in M′MOFs at 273 K and 1 atm. The calculated Henry C_2H_2/C_2H_4 separation selectivities in **HOF-1a** are 19.3 and 7.9 at 273 and 296 K, respectively, which are much higher than the values of 4.1 and 5.2 in the recently discovered **M′MOF-3a**. The adsorption enthalpies at zero coverage are 58.1 and 31.9 kJ mol^{-1} for C_2H_2 and C_2H_4, respectively. The high separation selectivity and stronger C_2H_2 binding might be attributed to the narrow pore space within **HOF-1a** and hydrogen bonding interactions of acidic H atoms of the guest acetylene molecules and the basic amine groups of **HOF-1a**.

Recently, Schröder and co-workers reported a hydroxyl-functionalized porous MOF **NOTT-300** that exhibits high selectivity and uptake capacity for acetylene/ethylene separation.[73] **NOTT-300** has a porous structure with channels formed by corner-sharing [$AlO_4(OH)_2$] octahedra bridged by tetracarboxylate ligands L^{4-} (H_4L = biphenyl-3,3′,5,5′-tetracarboxylic acid) *via* two mutually *cis*-μ_2-OH groups (Fig. 2). At 293 K and 1.0 bar, **NOTT-300** can adsorb C_2H_2 and C_2H_4 at a capacity of 6.34 and 4.28 mmol g^{-1}, respectively. The difference in the uptakes between C_2H_2 and C_2H_4 is 2.06 mmol g^{-1}, which is comparable to that observed in **HOF-1** (2.45 mmol g^{-1}) and **M′MOF-3a** (1.5 mmol g^{-1}) but significantly higher than that in **FeMOF-74** (0.7 mmol g^{-1}). The C_2H_2/C_2H_4 selectivity for equimolar

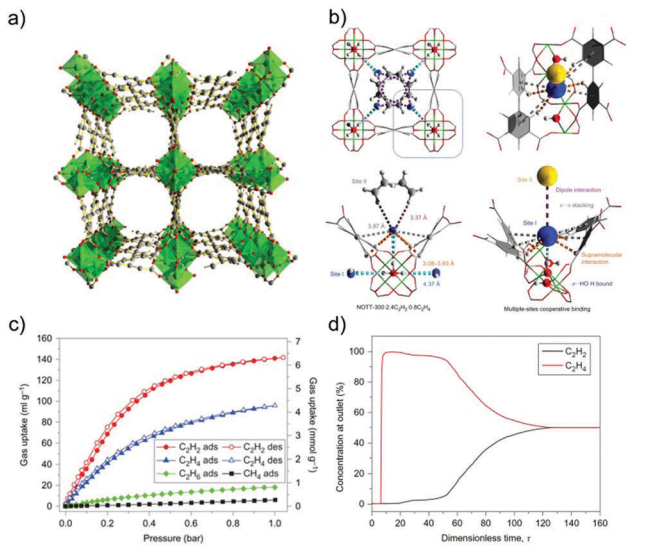

Fig. 2 (a) View of the 3D framework structure of **NOTT-300** along the *c*-axis. (b) Images of the structure of **NOTT-300**·2.4C_2H_2·0.8C_2H_4 obtained from DFT calculations based on INS spectra (Al, green; C, grey; O, red; H, white). The carbon atoms of C_2H_2 are highlighted in blue. Sites I and II represent two preferred binding sites within the pore, and are shown by blue and yellow balls, respectively. The π···HO hydrogen bonds, π···π stacking, C···H supramolecular interactions and intermolecular dipole interactions are highlighted in cyan, grey, orange and purple, respectively. (c) Adsorption isotherms of C_2H_2, C_2H_4, C_2H_6 and CH_4 in **NOTT-300** at 293 K. (d) Experimental breakthrough data for an equimolar mixture of C_2H_2/C_2H_4 in a fixed bed packed with **NOTT-300** measured at 293 K and 1.0 bar.[73]

mixtures at 1.0 bar was estimated to be 2.30 by IAST calculations on the basis of the pure-component isotherms at 293 K, outperforming **FeMOF-74** (1.87). Density functional theory (DFT) calculations and an inelastic neutron scattering (INS) study for competitive adsorption between these two molecules within **NOTT-300** suggest that the cooperative supramolecular interactions, *i.e.* the π···HO hydrogen-bonds, π···π stacking, C···H supramolecular interactions and intermolecular dipole interactions between acetylene and **NOTT-300**, account for the stronger binding energy for acetylene (30–32 kJ mol^{-1}) against ethylene (16–28 kJ mol^{-1}), which was found at the centre of the cavity within the framework and interacts predominantly with the acetylene molecules *via* electrostatic dipole interaction (Fig. 2). The highly selective acetylene/ethylene separation has also been confirmed in the breakthrough experiment using an equimolar mixture of C_2H_2/C_2H_4 on a packed bed of **NOTT-300** under ambient conditions, giving a C_2H_4 purity of 99.5%. Compared with the π-complexation between open metal sties and the π-electrons of C_2H_2 or C_2H_4 (typical isosteric adsorption heats of 40–60 kJ mol^{-1}), the soft binding nature of these supramolecular interactions could facilitate modest regeneration.[73]

Hu *et al.*[72] recently reported a microporous MOF Cu(ATBDC) (**UTSA-100**; H_2ATBDC = 5-(5-amino-1*H*-tetrazol-1-yl)-1,3-benzenedicarboxylic acid), which exhibits highly efficient removal of acetylene from ethylene/acetylene mixtures. **UTSA-100** has a three-dimensional framework with rhombic open zigzag nanochannels with amino and tetrazole functionalized walls. There are small cages with a diameter of about 4.0 Å connecting two adjacent 1D zigzag channels (diameter of 4.3 Å) with window openings of 3.3 Å (Fig. 3). At 296 K and 1 atm, the acetylene and ethylene uptake amounts of desolvated **UTSA-100** (denoted as **UTSA-100a**) are 95.6 and 37.2 $cm^3\ g^{-1}$, respectively. The C_2H_2/C_2H_4 uptake ratio of 2.57 in **UTSA-100a** is systematically higher than the most current state-of-the-art MOFs including **NOTT-300** and **MMOF-74** (M = Mg, Co, Fe). The breakthrough simulations for the C_2H_2/C_2H_4 (1 : 99, v/v) mixture demonstrated the superior performance of **UTSA-100a** in removing acetylene from ethylene/acetylene mixtures containing 1% acetylene owing to the collaboration of high adsorption selectivity and high uptake capacity. It is speculated that weak acid–base interactions between the $-NH_2$ of frameworks and acetylene molecules play important roles for the preferential binding of **UTSA-100a** with C_2H_2 over C_2H_4.[72]

Very recently, Cui and co-workers reported a series of coordination networks composed of inorganic anions of SiF_6^{2-} (hexafluorosilicate, **SIFSIX**), which exhibits unprecedented performance in the separation of C_2H_2/C_2H_4.[76] In these primitive cubic "**SIFSIX**" materials, pore walls lined by SiF_6^{2-} and pore size can be tuned by changing the size of the organic linkers. IAST calculations show that **SIFSIX-2-Cu-i** exhibits the record-high C_2H_2/C_2H_4 selectivity (39.7 to 44.8), higher than all these previously reported best-performing MOFs. At 298 K and 0.025 bar, **SIFSIX-2-Cu-i** (2 = 4,4′-dipyridylacetylene, i = interpenetrated) shows an exceptionally high C_2H_2 uptake capacity of 2.1 mmol g^{-1}, making **SIFSIX-2-Cu-i** the most suitable for C_2H_2/C_2H_4 (1/99) separations. **SIFSIX-1-Cu** (1 = 4,4′-bipridine) is the leading material for C_2H_2/C_2H_4 (50/50) separation, with a moderately high C_2H_2/C_2H_4 selectivity (7.1 to 10.6) and an exceptional C_2H_2 capture capacity of 8.5 mmol g^{-1} (298 K, 1.0 bar). DFT calculations and neutron powder diffraction experiments both confirmed that each unit cell of **SIFSIX-1-Cu** contains four C_2H_2 molecules through the cooperative host–guest (C–H···F H-bonding) and guest–guest interactions. In **SIFSIX-2-Cu-i**, each C_2H_2 molecule was bound by two F atoms from different nets (Fig. 4). The excellent recognition of these **SIFSIX** materials for C_2H_2 molecules was examined through experimental column breakthrough by mimicking actual industrial processes for both 1/99 and 50/50 C_2H_2/C_2H_4 mixtures.

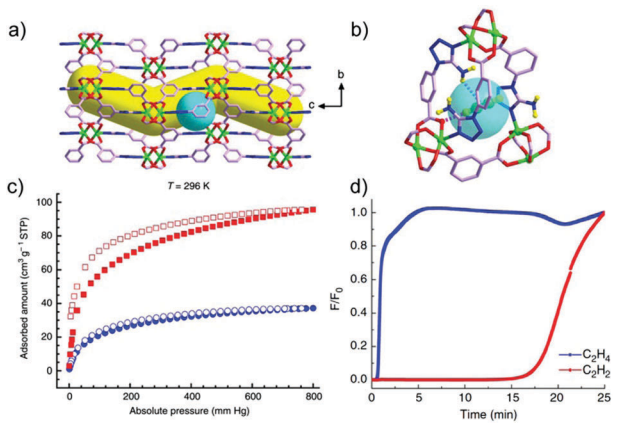

Fig. 3 (a) The pore structure of **UTSA-100** showing the zigzag channels along the *c* axis and the cage with a diameter of about 4.0 Å in the pore wall with window openings of 3.3 Å. (b) The acetylene sits right at the small cage connecting two adjacent channel pores. (c) Acetylene (red) and ethylene (blue) sorption at 296 K. Adsorption and desorption branches are shown with closed and open symbols, respectively. (d) Experimental column breakthrough curve for C_2H_2/C_2H_4 mixed gas containing 1% C_2H_2 over **UTSA-100a** at 296 K.[72]

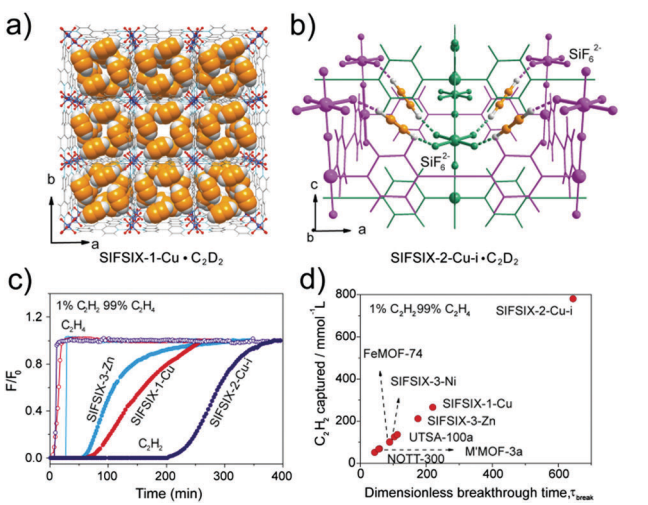

Fig. 4 Neutron crystal structure of **SIFSIX-1-Cu·C_2D_2** (a) and **SIFSIX-2-Cu-i·C_2D_2** (b) at 200 K from Rietveld analysis. (c) Experimental column breakthrough curves for C_2H_2/C_2H_4 separations (1/99). (d) Plots of the amount of C_2H_2 captured as a function of τ_{break} in the simulated column breakthrough for C_2H_2/C_2H_4 separations (1/99).[76]

2.3 Adsorptive separation of olefins over paraffins

Olefin/paraffin separations represent a class of the most energy-intensive separations carried out on a large scale in the petrochemical industry.[1] They continue to be the most difficult and the most costly distillation processes because of similar sizes and close relative volatilities (*e.g.* the difference in the boiling points of ethylene and ethane is 15 K, and the relative volatility is about 1.2. The difference in the boiling points of propylene and propane is 5.3 K, and the relative volatility is about 1.14). Industrially, ethylene–ethane separation is typically carried out at about −25 °C and 23 bar in a column containing over 100 trays, and the process for propylene–propane separation is performed by an equally energy-intensive distillation at about −30 °C and 30 bar.[77] An alternative olefin/paraffin separation process with low energy consumption would significantly reduce operating expenses. To date, a number of adsorbents have been evaluated for the adsorptive separation of olefin/paraffin mixtures, but only a very limited number of zeolites have shown the potential for the kinetically controlled separation of olefins and paraffins.[78–93] The development of new adsorbents with adequate selectivity and capacity is a key step for the efficient separation of these molecules. Emerging as a new family of porous adsorbent material, a few metal–organic frameworks have been reported to show great potential in these separations mainly by one or more of the following mechanisms: (1) the thermodynamic equilibrium effect; (2) kinetic effect; (3) gate-opening effect; and (4) molecular sieving effect.

2.3.1 Adsorption separation based on a thermodynamic equilibrium effect. Most effective separations of olefins and paraffins in metal–organic frameworks were achieved by thermodynamic equilibrium separations. Open metal sites within metal–organic frameworks play an important role in such separations. The first investigation into a metal–organic framework with open metal sites for the adsorptive separation of ethylene over ethane was performed on **$Cu_3(btc)_2$**. The structure of **$Cu_3(btc)_2$** is self-assembled by dimers of Cu(II), in which each copper atom is coordinated to four oxygen atoms from the btc ligands. In the as-synthesized form, Cu is coordinated to a water molecule axially. Under dehydration, Cu atoms release the coordinated water, leading to coordinatively unsaturated sites of Cu(II), which could play an important role in the adsorption of olefins. Preferential sorption of ethylene on **$Cu_3(btc)_2$** could be noticeably observed from the adsorption isotherm. The authors speculated that the adsorption properties are related to a specific interaction between the double bond in the ethylene molecule with the partially charged copper atoms in the framework.[94,95] Bhatia *et al.* investigated the interaction between ethylene/ethane and the framework by quantum mechanical calculations, and revealed that ethylene binds stronger than ethane as a result of stronger hydrogen bonding with the basic oxygen atoms as well as some degree of electrostatic interaction with copper atoms in the framework.[96] Grand Canonical Monte Carlo (GCMC) calculations show the isosteric heats at low loading are in the range of 22–30 kJ mol^{-1}, with a slight difference in isosteric heat found to be 3 kJ mol^{-1}, which leads to a theoretical selectivity of only *ca.* 2 for an equimolar ethylene/ethane mixture at 298 K.[97,98]

Like its performance in ethane/ethylene separations, **$Cu_3(btc)_2$** also preferentially binds propylene over propane considering the difference in isosteric heat at zero coverage (−41.8 kJ mol^{-1} for propylene *vs.* −28.5 kJ mol^{-1} for propane).[99] Rodrigues and co-workers demonstrated the feasibility of the separation of propane/propylene from both experimental measurements and molecular simulations. GCMC and DFT calculations suggested that the stronger preferential adsorption of propylene can possibly be attributed to the specific interaction between the π-bonding orbital in propylene molecules with the vacant s-orbital of the copper atom and that propane is adsorbed preferentially in the small octahedral pockets present in the framework.[99–102] This can also be confirmed by the observation of bathochromic shift on UV/Vis spectra because of propylene coordination with open copper metal sites. The separation performance of **$Cu_3(btc)_2$** was further verified by binary breakthrough experiments, which illustrated the separation factors of propylene over propane ranging from 3.3 (at 313 K) to 5.5 (at 353 K).[103] Inspired by the promising results for olefin/paraffin separations, **$Cu_3(btc)_2$** materials with a variety of morphologies including spheres,[104,105] tablets[106] and extrudates[107] have been evaluated extensively for the potential application in pressure swing adsorption (PSA), vacuum swing adsorption (VSA) or simulated moving bed (SMB) processes.

Additionally, the potential of **$Cu_3(btc)_2$** for the separation of isobutane and isobutene has also been investigated.[108] Similarly, adsorption isotherms at temperatures ranging from 303 to 323 K display a somewhat higher amount of isobutene as compared to isobutane. Nevertheless, differential enthalpies of adsorption differ only by about 5 kJ mol^{-1}, giving a modest separation factor of 2.1 that was confirmed by a binary breakthrough experiment using an equimolar mixture of isobutane and isobutene at 303 K.[108]

Since the open metal sites play an important role in enhancing the selectivity of MOF materials,[109] **MIL-100(Fe)** featuring the structural characteristics of coordinatively unsaturated sites is also capable of separating propane/propylene mixtures.[110–113] Yoon *et al.* reported that creating open Fe^{II} sites in the dehydrated **MIL-100(Fe)** could lead to a strong improvement in the selective adsorption of unsaturated gas molecules such as propylene and CO. Interestingly, the adsorption affinity for propylene and propane were relevant to the valence of the iron centers, which is dependent on the activation temperature. Partial open Fe^{II} sites could be generated by activation under high vacuum at temperatures ranging from 423 to 523 K owing to the departure of anionic ligands (F^- and OH^-). The adsorption heat of propylene dramatically and negatively increased from the initial −30 kJ mol^{-1} up to −70 kJ mol^{-1} in the presence of open Fe^{II} sites while that of propane remains the same (−30 kJ mol^{-1}). The preferential adsorption affinity towards propylene may mainly be ascribed to the π-back donation interaction between the open Fe^{II} sites and the C=C entities in propylene, which has been clearly evidenced by infrared spectroscopy and microcalorimetry.[112,113] Breakthrough experiments with an equimolar binary mixture at 2.5 kPa gave a separation factor of 28.9 for propylene over propane at 40 °C. Remarkably, though the separation factor decreased by 10.8 at

5 kPa, it is still at least three times higher than that in $Cu_3(btc)_2$.[111] The presence of open Fe^{II} sites can dramatically improve the separation performance as a result of its softer metal character. Analogous to **MIL-101(Fe)**, open Cr(III) metal sites in **MIL-101** binds ethylene over ethane with modest theoretical selectivity between 4 and 6 based on IAST prediction for an equimolar mixture.[114]

The series of **MMOF-74** materials, also denoted as M_2**(dobdc)** (dobdc = 2,5-dioxido-1,4-benzene-dicarboxylate) or **CPO-27-M**, are another archetypal example of MOFs with high-density open metal sites (7.13–7.58 mmol M^{2+} per cm^3), and perform exceptionally well for the olefin/paraffin separations.[77,115,116] Bao *et al.* reported the first example of **MgMOF-74** for ethane/ethylene and propane/propylene separations.[77] Although this material displays similar saturation capacities for ethane/ethylene and propane/propylene pairs at a given temperature, the isosteric heat of adsorption at zero coverage for either ethylene or propylene is much higher than that of the saturated counterparts. The adsorption selectivities for ethane/ethylene and propane/propylene separations were estimated to be up to *ca.* 15 and *ca.* 19, respectively. As expected, GCMC simulations reveal that all adsorbates were preferentially adsorbed by the open Mg^{2+} sites and that each site is occupied by one molecule.[77] Subsequently, Snurr and co-workers systematically examined the adsorption selectivities of propene over propane on a series of isostructural frameworks **MMOF-74** (M = Co, Mn, and Mg). **CoMOF-74** (*ca.* 46) shows substantially higher selectivity than **Mn-MOF-74** (*ca.* 24) and **MgMOF-74** (*ca.* 4.5) because of the strongest propylene binding to Co^{2+} sites. Breakthrough experiments on an equimolar mixture of propylene and propane in a packed column of **CoMOF-74** further confirmed this highly efficient separation.[117] In terms of the volumetric capacity, **NiMOF-74** has the highest capacity towards olefins. Zhu and co-workers demonstrated the potential of **NiMOF-74** for the separation of a propane/propylene mixture by the experimental transient breakthroughs in a fixed bed.[118] For propane and propylene separation, the **MgMOF-74**-based fixed bed is more feasible to separate them than membrane permeation because the higher permeability of propane through the 1D pore system counteracts the dominant adsorption uptake of propylene over propane.[119]

Compared to the other extensively investigated isostructural **MMOF-74** (M = Co, Mn, Ni, Mg, and Zn), **FeMOF-74** performs even better for ethane/ethylene and propane/propylene separations because of the softer metal character of open Fe^{2+} cation sites exposed on its surface. Long and co-workers demonstrated that **FeMOF-74** is capable of separating ethylene/ethane and propylene/propane mixtures at 318 K with excellent performance.[66] For an equimolar mixture of ethylene and ethane at 318 K, the adsorption selectivities obtained for **FeMOF-74** of 13 to 18 are significantly greater than those obtained for either zeolite NaX or the isostructural **MgMOF-74**, which display selectivities of 9 to 14 and 4 to 7, respectively. Moreover, the uptake of these gases at 1 bar approaches the stoichiometric quantity expected if one gas molecule is adsorbed per iron(II) center (Fig. 5). Breakthrough experiments show that this material can separate an equimolar ethane/ethylene mixture at 1 bar and 318 K into the pure component gases of 99% to 99.5% purity. As for an equimolar propylene–propane gas mixture, 100% pure propane and greater than 99% propylene could be obtained. Furthermore, the breakthrough simulations indicate that the production capacities for ethylene/ethane separation are roughly double those of **MgMOF-74** and zeolite NaX. For propane/propylene separation, the propane production capacity at 318 K is at least 20% higher than that of any other material including NaX, ITQ-12, $Cu_3(btc)_2$, and **MIL-100(Fe)**. Neutron powder diffraction experiments confirm that the open coordination site of the exposed Fe^{2+} cations is indeed the primary adsorption site. The unsaturated hydrocarbons acetylene, ethylene, and propylene were adsorbed *via* the anticipated side-on binding mode with Fe–C distances in the range of 2.42 to 2.60 Å, while the interactions of both ethane and propane with metal cations are even weaker with the elongated Fe–C distance of ~3 Å.[66] In the follow-up study, Long and co-workers investigated how the adsorption performance for olefin/paraffin separations changed with a variation in the framework metal cations. For all **MMOF-74** materials, the selectivity of propylene over propane is higher than

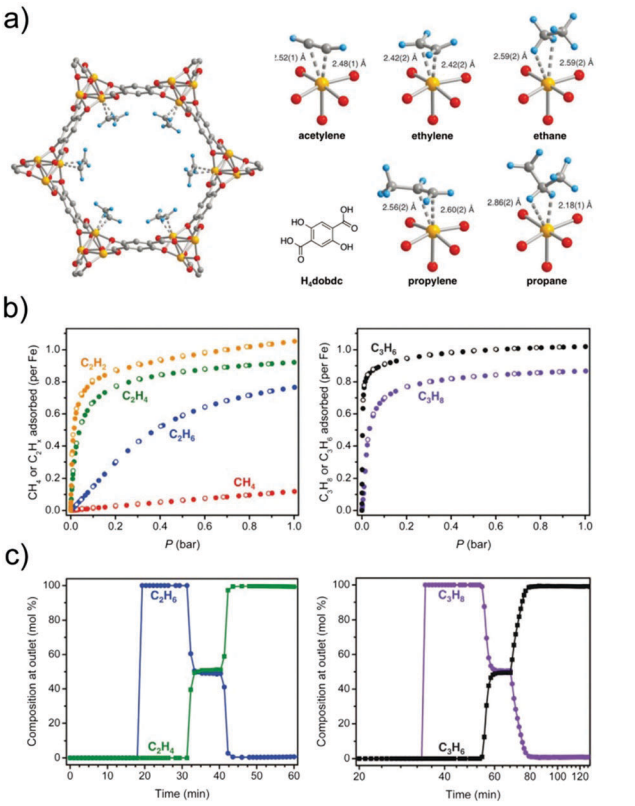

Fig. 5 (a) Left: A portion of the solid-state structure of Fe_2**(dobdc)**·$2C_2D_4$ as determined by the analysis of neutron powder diffraction data; orange, red, gray, and blue spheres represent Fe, O, C, and D atoms, respectively. Right: H_4(dobdc) ligand and the first coordination spheres for the iron centers in the solid-state structures obtained upon dosing Fe_2**(dobdc)** with acetylene, ethylene, ethane, propylene, and propane. (b) Gas adsorption isotherms for methane, ethane, ethylene, and acetylene (left) and propane and propylene (right) in Fe_2**(dobdc)** at 318 K. (Filled and open circles represent adsorption and desorption data, respectively.) (c) Experimental breakthrough curves for the adsorption of equimolar ethane/ethylene (left) and propane/propylene (right) mixtures flowing through a 1.5 mL bed of Fe_2**(dobdc)** at 318 K with a total gas flow of 2 mL min^{-1} at atmospheric pressure.[66]

that of ethylene over ethane. Among all tested MOFs, **FeMOF-74** has the highest selectivity for ethylene–ethane at all mixture compositions, while **MnMOF-74** shows the greatest selectivity for propylene–propane. The Mg and Zn-based analogues exhibit the lowest selectivities for both separations primarily due to the weaker interactions between these metal cations and the unsaturated hydrocarbons.[120] Unfortunately, the alkene/alkane selectivity in a series of **MMOF-74** frameworks relies on the strong binding of unsaturated hydrocarbons to open metal sites, and these materials easily lose their activity rapidly on exposure to moisture.[121–123] This instability is the major disadvantage hindering their practical application.

It has been well-established that some transition metals such as Cu(I) and Ag(I) ions can form π-complexes with the carbon–carbon double bonds of olefin molecules to enforce and differentiate their interactions with olefin from paraffin.[124–126] Bao and Chen introduced Ag(I) ions into a sulfonic acid functionalized MOF (**(Cr)-MIL-101-SO$_3$H**), significantly enhancing its interactions with olefin double bonds, and leading to very high selectivities for the separation of ethane–ethylene and propane–propylene at room temperature.[127] For an equimolar mixture of ethylene and ethane at 303 K, the adsorption selectivity obtained for **(Cr)-MIL-101-SO$_3$Ag** is 16 at 100 kPa, apparently greater than those for most zeolites and MOFs reported. Particularly, at low pressures, its adsorption selectivity at 1 kPa of 238 is nearly twice that recently reported for **PAF-1-SO$_3$Ag** (125 at 296 K),[128] and is the highest ever reported for the adsorptive separation of ethylene–ethane mixtures. Simultaneously, Ma and co-workers found that the ethylene–ethane adsorption selectivity of **(Cr)-MIL-101-SO$_3$Ag** at 318 K and 100 kPa (9.7) is also significantly higher than those of the zeolite NaX, **MMOF-74** (M = Co, Mg) and **Cu$_3$(btc)$_2$** because of more efficient π-complexation.[129] In addition, loading transition metal ions inside the porous matrices of MOFs is also an effective approach to enhance the olefin/paraffin adsorption selectively. Chang *et al.* demonstrated a MOF composite by dispersing CuCl nanoparticles inside the pores of **MIL-101** to improve the ethane/ethylene separation. The **MIL-101** with 40 wt% loading of CuCl shows a significantly enhanced ideal adsorption selectivity of ethylene over ethane up to 14.0 against that of 1.6 on the parent **MIL-101**. This may be attributed to the newly generated Cu^+ sites that can selectively interact with the C=C bond in ethylene through π-complexation.[130]

Another example of MOFs with olefin/paraffin adsorption selectivity based on π-complexation is **Ag$_2$[Cr$_3$O(OOCCH$_2$CH$_3$)$_6$(H$_2$O)$_3$]$_2$[α-SiW$_{12}$O$_{40}$]**, which is a flexible framework composed of 2D-layers of polyoxometalates $[\alpha\text{-}SiW_{12}O_{40}]^{4-}$ and macrocations $[Cr_3O(OOCC_2H_5)_6(H_2O)_3]^+$, and Ag^+ ions.[131] This material can selectively adsorb small unsaturated hydrocarbons such as ethylene, propylene, *n*-butene, acetylene, and methyl acetylene with the uptake no less than 1.0 mol mol^{-1}, while paraffins and larger unsaturated hydrocarbons such as isobutene and *n*-pentene were almost completely excluded because of difficulty in penetrating into the solid bulk. Remarkably, the sorption ratios of ethylene/ethane and propylene/propane are over 100 at 298 K and 100 kPa. Detailed research revealed that this selectivity may be attributed to the effective penetration of small unsaturated hydrocarbons into the framework through π-complexation with Ag^+.[131] Thereafter, the same group synthesized two porous ionic crystals $Ag_2[Cr_3O(OOCCH_2X)_6(H_2O)_3]_2[\alpha\text{-}SiW_{12}O_{40}]$ (X = Cl or Br) by complexation of halogen-substituted macrocations with a silicododecatungstate. They could selectively adsorb olefins over paraffins. Propylene/propane and ethylene/ethane sorption ratios on the dehydrated former at 298 K and 100 kPa are 6.1 and 3.6, respectively, and the ethylene/ethane sorption ratio on the latter at 298 K and 100 kPa is 2.8. Detailed research demonstrated that the preferential olefin sorption could be ascribed to the electrostatic interaction between the π-electron of olefins and highly polarized halogen-substituted macrocations and/or silicododecatungstates.[132]

According to the recent work of Schröder's group, **NOTT-300** seems to be the leading ethylene/ethane separating material, which shows the highest IAST ethylene/ethane selectivity (48.7) reported so far. The high selectivity may be ascribed to the difference in the supramolecular interactions of guest molecules within the **NOTT-300** host. DFT calculations and INS spectra reveal that C_2H_6 has very weak interactions with the **NOTT-300** host, while π···HO hydrogen bonds and the π···π stacking interaction between C_2H_4 molecules and the framework yields the stronger binding of C_2H_4 to **NOTT-300**. In contrast to MOF materials with open metal sites, **NOTT-300**, with soft functional groups and coordinatively saturated Al(III), might be more promising in practical adsorption applications performed under humid conditions.[73]

For most MOF materials, olefins are more likely to coordinate with metal ions in the framework, and thus the desired olefin product could be only obtained during the desorption stage. Very recently, the Chen group at Sun Yat-Sen University reported an exceptional adsorption behavior on a porous metal-azolate framework **MAF-49** [Zn(batz), H$_2$batz = bis(5-amino-1*H*-1,2,4-triazol-3-yl)methane] that can bind ethane much stronger than ethylene, making it particularly useful for the production of high-purity ethylene.[133] **MAF-49** is a three-dimensional coordination framework with an ultra-microporous 1D zigzag channel (3.3 Å × 3.0 Å), which is comparable with the kinetic diameters of ethane and ethylene. The surfaces of these channels are rich with electronegative nitrogen atoms from the bistriazole ligand, which tender plentiful hydrogen-bonding acceptors (Fig. 6). Single-crystal X-ray diffraction and GCMC simulations revealed that the exceptionally high ethane/ethylene selectivity might arise from the suitable positioning of multiple electronegative and electropositive functional groups on the pore surface, which allows multiple hydrogen-bonding interactions with ethane but fewer and weaker attractive interactions for ethylene. The practical separation performance of **MAF-49** has been investigated by breakthrough experiments at 313 K and 1 bar. Breakthrough experiments using a typical cracked gas mixture (15 : 1 ethylene/ethane) showing a single **MAF-49** column could directly produce 56 times column volume of ethylene with polymerization purity over 99.95% at the outlet with a single breakthrough operation, outperforming other ethane-selective materials including **MAF-3**, **MAF-4** and **IRMOF-8**.[133]

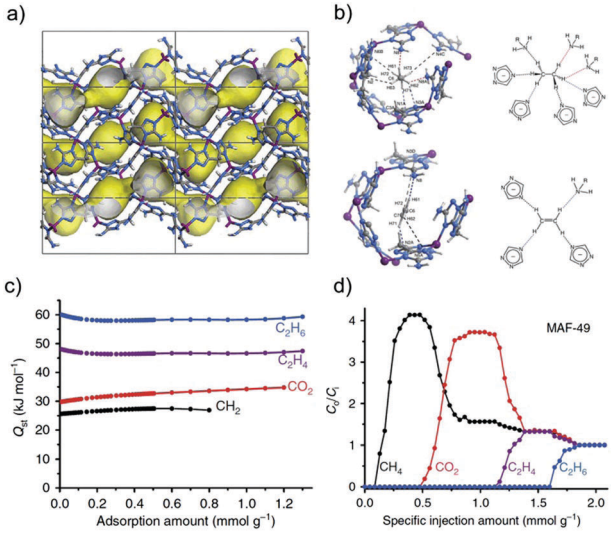

Fig. 6 (a) Crystal structure of **MAF-49**. (b) Preferential adsorption sites for ethane and ethylene in **MAF-49** revealed by computational simulations. (c) The coverage-dependent adsorption enthalpy for ethane, ethylene, carbon dioxide and methane. (d) Breakthrough curves of four-component equimolar gas mixture (CH_4/CO_2/C_2H_4/C_2H_6) separation on **MAF-49**.[133]

2.3.2 Diffusion selective separations of olefin/paraffin mixtures. Li and co-workers reported the first examples of microporous metal organic frameworks (MMOFs) that are capable of kinetic separation of propane and propylene.[134] The promising kinetic selectivity of propylene over propane was observed on three isostructural ZIFs, namely **Zn(2-cim)$_2$** (2-cim = 2-chloroimidazolate), **Zn(2-bim)$_2$** (2-bim = 2-bromoimidazolate), and **ZIF-8**. Under equilibrium conditions, **ZIF-8** revealed essentially identical adsorption uptake of propylene and propane, and their isosteric adsorption heats at low loadings are also similar, indicating that thermodynamic separation seems to be impractical. However, the single-component diffusion studies reveal that the kinetic separation of propylene and propane by these ZIFs should be highly probable based on the remarkable differences in their diffusion rates through the pore systems. For example, at 30 °C, the ratios of diffusion rates of propylene over propane through **ZIF-8** and **Zn(2-cim)$_2$** are 125 and 60, respectively (Fig. 7). The effective size of the pore opening in these MOFs is the controlling factor determining the separation capability.

Owing to the significant diffusion difference especially between paraffins and olefins, **ZIF-8** has become one of the most popular MOFs for fabricating mixed-matrix membranes for their separations.[135–158] For membrane separation, the knowledge of the transport diffusivities of light hydrocarbons across the membrane is sometimes more important than the adsorption capacity performance.[138,145–147,156,159,160] Both computational and experimental studies have confirmed that the ethane/ethylene selectivity in **ZIF-8** is quite limited.[135,137,149] For example, **ZIF-8** membranes fabricated by Bux *et al.* separate an equimolar ethylene/ethane mixture at room temperature and 1 and 6 bar feed pressure with a selectivity of 2.8 and 2.4, respectively.[135] The high-quality **ZIF-8** based membranes showed

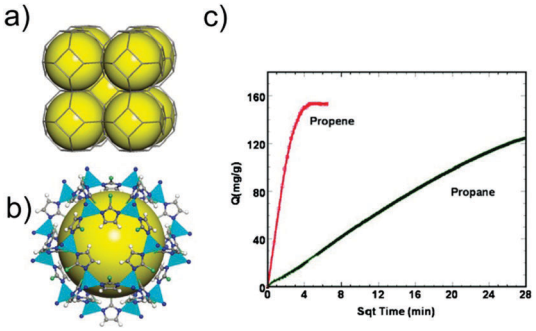

Fig. 7 (a) Expanded sodalite framework topology formed by connecting the tetrahedral Zn^{II} centers. (b) View of the pore opening along the three-fold axis of **ZIF-8**. C: gray; H: white; N: blue; Zn: light blue. (c) Propylene and propane uptake by **ZIF-8** as a function of the square root of time.[134]

exceptionally high separation performance of an equimolar propylene/propane mixture with permeability selectivity around 55 at room temperature.[158] Interestingly, although the effective aperture size of **ZIF-8** for molecular sieving falls in the range of 4.0 to 4.2 Å, the C4 hydrocarbon molecules considerably larger than the effective aperture size range are still able to diffuse into the micropores of **ZIF-8** with the kinetic selectivities for iso-C_4H_8/iso-C_4H_{10} of 180 and *n*-C_4H_{10}/iso-C_4H_{10} up to 2.5 × 10^6 at 308 K. It is believed that the combination of aperture flexibility and dilation may explain the observed kinetic effect.[161]

Hupp and co-workers reported the kinetic separation of propane and propylene in another series of isostructural MOFs shown in Fig. 8.[162] These noncatenated, pillared-paddlewheel MOFs with 3D pores are made up of dipyridyl struts and tetracarboxylate struts held together with Zn^{2+} nodes. The single crystals of these MOFs were isolated as highly anisotropic rectangular plates that are thin along the direction of the dipyridyl ligands. The MOF crystals favor the motion of propane and propylene through the I and II channels (Fig. 8a and b) and terminate on the largest crystal faces (the top-to-bottom channels) because the combined area of the four edge faces is much smaller than that of the top and bottom faces. The apertures of top-to-bottom channels can be tuned by 3,6-functionalization of the tetracarboxylate ligands, while the apertures of edge channels can be modulated by the functionalization of dipyridine ligands. Both modifications allowed the researchers to examine the effect of pore apertures on the kinetic separation of propylene and propane in this system. The kinetic adsorption selectivity for propylene *versus* propane was deduced from the time-dependent gas uptake profiles (Fig. 8c). It was found that DBTO and BTO with Br moieties showed much higher kinetic selectivities than those of corresponding TO and DTO without Br moieties. In view of the thin rectangular plate morphology of the MOF crystals, the large kinetic selectivities for propylene over propane observed in DBTO and BTO could be best attributed to the reduction in the apertures of channels I and II, which efficaciously discriminated the transport of both molecules with close size. This explanation was further supported by the decreased kinetic selectivity observed in a ground sample of DBTO because of the reduced plane of the top-to-bottom channels.

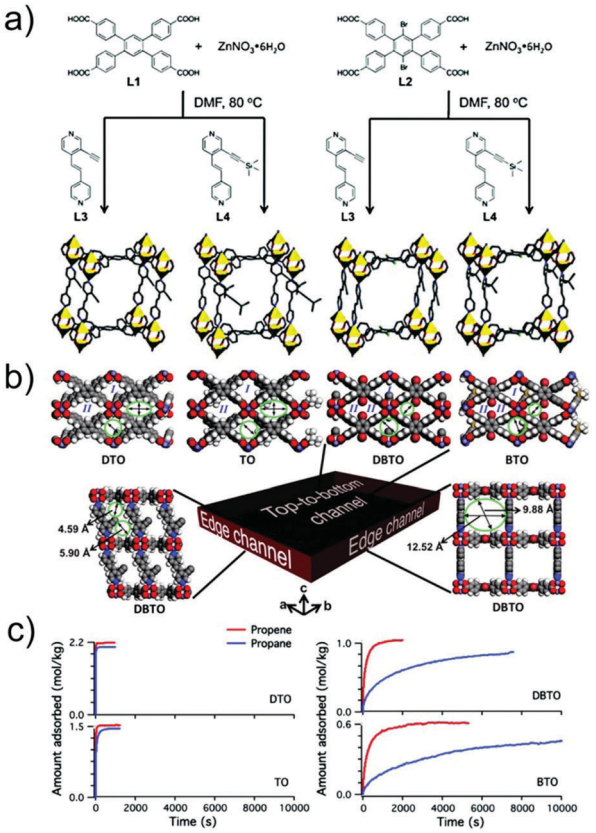

Fig. 8 (a) Synthesis, structures, and crystal packing diagrams of the four isostructural MOFs DTO, TO, DBTO, and BTO (the stick representation of the unit cell for each MOF is shown (yellow polyhedra = Zn, red = O, green = Br, blue = N, gray = C; solvent molecules, hydrogen atoms, and disordered atoms have been omitted for clarity)). (b) Crystal-packing diagrams of DBTO showing the framework pores along the *a* (right) and *b* (left) axes. (c) Time-dependent propylene and propane uptake profiles for DTO, TO, DBTO, and BTO MOFs at 0.3 bar and 298 K.[162]

2.3.3 Separations based on a gate-opening effect. From a practical point of view, it is preferable to recover the desired alkene product in the adsorption step because the desired alkene product, required for the production of polymer grade polyethylene and polypropylene, can only be recovered in the desorption phase once using alkene-selective adsorbents. Generally, the binding energy of the alkenes, especially with the coordinatively unsaturated metal sites, is significantly higher than that of the saturated alkanes. The energy requirements for the desorption and regeneration processes are high as the alkene product with the desired purity is recovered in the final step. Therefore, using alkane-selective adsorbents may accomplish adsorptive olefin/paraffin separations with fewer cycles and less energy. However, there are only a few MOFs that present the preferential adsorption of paraffins over olefins.[133,163–165] Among these MOFs, the aforementioned **MAF-49** is the best example of adsorptive separations that favour saturated ethane over unsaturated ethylene.[133]

Gascon and co-workers demonstrated the first example of a microporous material **ZIF-7** (Zn_2(bim), bim = benzimidazole) displaying a strong preferential adsorption of ethane over ethylene.[164] In contrast to most microporous materials, the inverse adsorption selectivity for paraffin may be attributed to a gate-opening effect in which specific opening pressures control the uptake and release of individual molecules (Fig. 9). The difference in gate-opening pressures for paraffins and olefins was determined by the interaction between guest molecules and the bim ligand in the narrow **ZIF-7** windows, which selectively discriminate the adsorption of both molecules with similar sizes but different shapes. Efficient separation of ethane and ethylene by **ZIF-7** was further confirmed by breakthrough experiments of the gas mixture.[164] In a follow-up study by the same group, the adsorption isotherms show that the ZIF structure opens or closes at different pressures depending on the adsorbate, and the structure opens at higher pressure with increasing temperature. DFT calculations revealed that the main difference in the behavior of alkenes and alkanes towards adsorption on **ZIF-7** is related to the ability of these molecules to form adsorption complexes at the external surface of the adsorbent window.[166] The effects of temperature and pressure on the behaviors of breakthrough experiments on **ZIF-7** were investigated by Zhu and co-workers.[167] The analysis of the experimental breakthroughs shows that an increase in temperature from 298 to 323 K slightly reduces the adsorption selectivity, while increasing pressure enhances the adsorption selectivity, which could be ascribed to the fact that the adsorbed ethylene molecules are replaced with adsorbing ethane molecules due to the higher adsorption affinity for ethane in **ZIF-7**.[167]

Another example of a flexible framework material **Zn_2(bpdc)$_2$(bpee)** (bpdc = 4,4′-biphenyldicarboxylate, bpee = 1,2-bipyriylethylene) that can separate ethylene from ethane based on a gate-opening mechanism was reported by Chabal and co-workers.[168] A pronounced gate-opening behavior, followed by stepwise isotherms with a strong hysteresis, is observed for both olefins and paraffins, with a clear dependence of the gate-opening pressure on the chain length. Raman spectroscopy and DFT calculations show that ethane interacts nonspecifically through its CH_3 group with the noncoordinated C═O bond of the framework, while there is a notable H-bonding effect between the CH_2 of the ethylene and the monodentate C═O bond of the ligand. It is believed that the gate-opening pressure is dependent on the hydrogen bonding

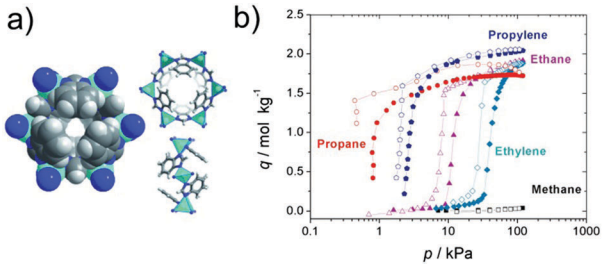

Fig. 9 (a) The main cavity entrance of **ZIF-7** together with the lateral and front view of one of the six-membered ring pore openings; Zn–N4 clusters are represented as polyhedra. (b) Adsorption (closed symbols)–desorption (open symbols) isotherms of several hydrocarbons on **ZIF-7** powder at 25 °C.[164]

strength between the terminal groups and the C=O bond of the bpdc ligand of the framework, and stronger H-bonding could lead to a lower gate-opening pressure.[168]

Kitagawa and co-workers also reported the selective adsorption of ethylene over ethane on a flexible **CPL-1** $[Cu_2(pzdc)_2pyz]$ (pzdc = 2,3-pyrazinedicarboxylate; pyz = pyrazine) based on a gas-induced structural change.[169] **CPL-1** preferentially adsorbs ethylene significantly more than ethane under ambient conditions because the threshold pressure of ethylene is apparently lower than that of ethane at the same temperature. Infrared spectroscopy and theoretical calculations suggest that hydrogen bonding between these gases and the carboxylate groups of the pzdc ligands of the framework is the dominant effect governing the selective sorption of the olefin. However, this framework suffers from a low ethylene uptake capacity (only 23 $cm^3\ g^{-1}$ at 273 K), although the selectivity was up to 3.8 as determined by breakthrough experiments.[169] Meanwhile, Kitagawa's group also evaluated the feasibility of ethylene/ethane separation on four two-fold interpenetrated mixed-ligand MOFs **$[Zn_2(tp)_2(bpy)]$**, **$[Zn_2(fm)_2(bpe)]$**, **$[Zn_2(fm)_2(bpa)]$**, and **$[Zn_2(fm)_2(bpy)]$** (tp = terephthalate, bpy = 4,4′-bipyridyl, fm = fumarate, bpe = 1,2-di(4-pyridyl)ethylene and bpa = 1,2-di(4-pyridyl)ethane). The structural transitions induced by the adsorption of ethylene and ethane were observed on these flexible frameworks except **$[Zn_2(fm)_2(bpy)]$**. Notably, there is a significant difference in the gate-opening pressure between ethane and ethylene only on **$[Zn_2(fm)_2(bpy)]$** with the smallest pores probably because ethylene molecules could be more specifically confined in the geometrically restricted pores. The ethylene/ethane separation on **$[Zn_2(fm)_2(bpy)]$** was further confirmed by breakthrough experiments using an equimolar ethylene/ethane mixture at 273 and 298 K.[170]

Very recently, a structurally flexible copper-based MOF showed that the gate-opening behaviour or structural transitions could be influenced by temperature, the chain length of the alkanes/alkenes and their bonding nature with the MOF material. The gate-opening effect might enable it to separate *n*-butane/1-butene mixtures to yield pure 1-butene at 273.15 K, but it showed less selectivity at higher temperature. The calculated breakthroughs suggested that ethylene/ethane/propane/*n*-butane/1-butene gas mixtures could be separated into three fractions with different carbon numbers.[171] Although another flexible MOF **$[Cu(dhbc)_2(4,4'\text{-bipy})]$** (dhbc = 2,5-dihydroxybenzoic acid) with gate-opening characteristics for C2/C3 hydrocarbon adsorption is incapable of separating olefins from paraffins, it however exhibits selective adsorption of propyne from a C1/C2/C3 mixture of hydrocarbons.[172]

2.3.4 Separation based on molecular sieving effects. Olefin/paraffin selectivity can also be achieved by precisely controlling the pore aperture size to provide molecular sieving. Very recently, Cadiau *et al.* demonstrated a complete molecular exclusion of propane from propylene at ambient temperature and atmospheric pressure using a fluorinated porous MOF material, **NbOFFIVE-1-Ni** (also referred to as **KAUST-7**).[173] The three-dimensional MOF material with square-shaped windows was constructed by bridging Ni(II)-pyrazine square-grid layers with $(NbOF_5)^{2-}$ pillars. Compared to another similar pillar-structured

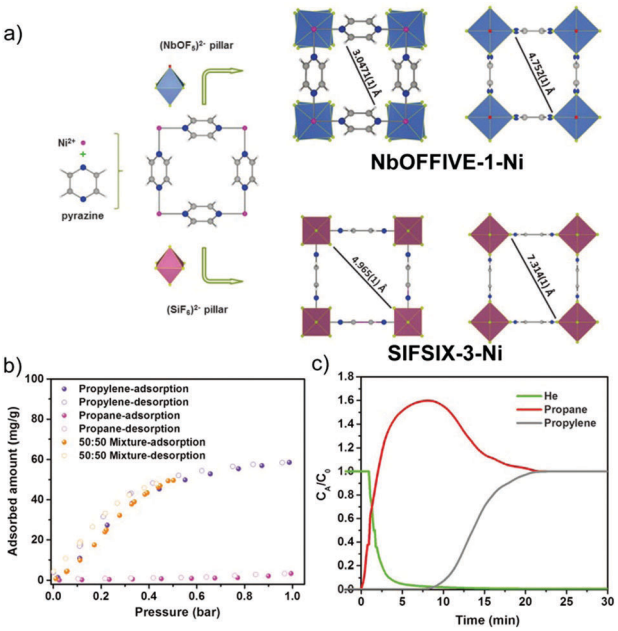

Fig. 10 (a) Structure description of **NbOFFIVE-1-Ni** highlighting the building block arrangement and its comparison with the parent **SIFSIX-3-Ni**. (b) The pure propane (pink), pure propylene (purple), and equimolar propylene/propane mixture (orange) isotherms of **NbOFFIVE-1-Ni** collected at 298 K and 1 bar. (c) Experimental breakthrough curves for the adsorption of an equimolar propylene/propane mixture flowing through a bed of **NbOFFIVE-1-Ni** at 298 K and 1 bar and 4 mL min^{-1} total flow.[173]

MOF (**SIFSIX-3-Ni**), the bulkier $(NbOF_5)^{2-}$ caused the steric hindrance between the pyrazine molecules and $(NbOF_5)^{2-}$ pillars, providing the smaller pore aperture size of 3.047 Å *versus* 5.032 Å in **SIFSIX-3-Ni** (Fig. 10a). The restricted aperture size opening owing to the hindered rotation of pyrazine ligands allows diffusion of the smaller propylene molecules into the pore system, but excludes the slightly bulkier propane. Thus, this MOF shows unprecedented propylene–propane selectivity by fine-tuning the pore size. The complete molecular sieving of propylene and the negligible adsorption of propane were further confirmed by gas adsorption isotherms, breakthrough and calorimetric–gravimetric experiments.

3. Adsorptive separation of linear and branched alkane isomers

The separation of linear, mono-branched, and di-branched isomers of alkanes is of significant importance in the petroleum industry. The di-branched alkanes in the 5–7 carbon number range are major components in high-octane gasoline because they have the relatively high values of Research Octane Number (RON), which usually increases with the degree of branching.[174,175] For example, di-branched hexane isomers 2,3-dimethylbutane (23DMB) and 2,2-dimethylbutane (22DMB) have RON values of 101.7 and 91.8, respectively. The RONs for the mono-branched isomers 2-methylpentane (2MP) and 3-methylpentane (3MP) are substantially lower, at 73.4 and

74.5, respectively, whereas the value for linear *n*-hexane (nHEX) is only 24.8 (Table 1).

Catalytic isomerization of linear alkanes as feedstock, for the purpose of octane improvement, is usually incomplete due to the limitation by thermodynamic equilibrium, and the product from the isomerization reactor commonly consists of an unreacted linear alkane along with its mono-branched isomers and di-branched isomers. Fig. 11 shows an example of a process for the isomerization of linear nHEX. To achieve higher octane number blends, an improved separation process would selectively isolate the most valuable products, 23DMB and 22DMB, meanwhile returning the less valuable nHEX and mono-branched isomers to the isomerization reactor (Fig. 11b). In current industrial practice, linear nHEX is separated from branched hydrocarbons using the zeolite 5A, which could only selectively adsorb linear nHEX but fails to separate di-branched alkanes from mono-branched ones.[176] To overcome this drawback, there is a crucial need to search for alternative sorbents that are able to more selectively adsorb di-branched alkanes from the mono-branched and linear ones.

To date, with the wide variety of MOFs currently available, some have shown promising results for the separation of linear alkanes from their branched isomers.[174–193] Li and co-workers[194] reported an ultra-microporous MOF **Cu(hfipbb)-(H_2hfipbb)$_{0.5}$** (H_2hfipbb = 4,4′-(hexafluoroisopropylidene)-bis(benzoic acid)) for the adsorptive separation of linear alkanes from branched alkanes in an early publication. This MOF has a 3D framework structure containing micro-channels with interconnected large elliptic chambers by small necks. This chamber space is slightly longer than the length of *n*-C4 (~6.9 Å), but just less than the length of *n*-C5 (8.1 Å), and the diameter of the neck is approximately 3.2 Å, which is too small to accommodate branched alkanes with diameters of around 3.9 Å. Thus, the micro-channels are able to separate linear C2–C4 hydrocarbons from all branched alkanes and all normal hydrocarbons above C4 (*e.g.* 2-methylpropane, *n*-pentane, 3-methylbutane, *n*-hexane, and 3-methylpentane). The first example for the separation of hexane isomers in the microporous MOF was reported by Chen and co-workers.[177] A microporous MOF, **Zn_2(bdc)$_2$(bpy)** (**MOF-508**, bdc = 1,4-benzenedicarboxylic acid; byp = 4,4′-bipyridine), has been demonstrated as the stationary phase for the gas-chromatographic (GC) separation of the linear and branched isomers of pentane and hexane (Fig. 12). This framework has a doubly interpenetrated 3D pillared-layer structure with a 4 Å × 4 Å cross section of 1D channels, which could selectively accommodate linear alkanes and discriminate branched alkanes. In a five-component breakthrough experiment, *n*-pentane can be easily separated from *n*-hexane and their respective isomers including 2-methylbutane, and 2-methylpentane and 2,2-dimethylbutane with this microporous MOF column. The efficient separation of alkanes within the **MOF-508** was believed to be a result of different van der Waals interactions arising from subtle size- and shape-selective matching.

Table 1 Molecular dimensions and research octane numbers of hexane isomers

Alkane	Boiling point (K)	Kinetic diameter (Å)	RON
n-Hexane	341.88	4.3	24.8
2-Methylpentane	333.40		73.4
3-Methylpentane	336.40	5.0	74.5
2,2-Dimethylbutane	322.87	6.2	91.8
2,3-Dimethylbutane	331.12	5.6	101.7

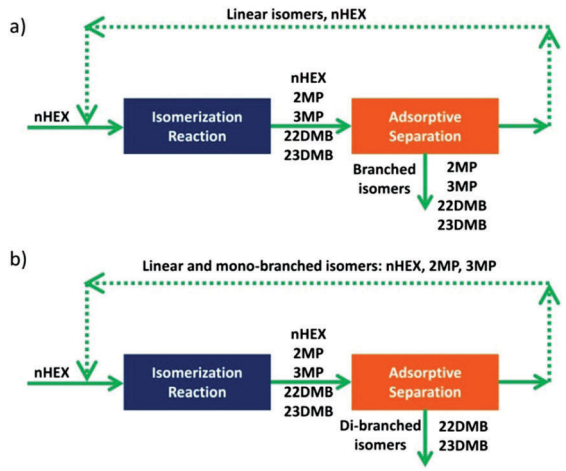

Fig. 11 (a) Conventional process flow scheme for alkane isomerization. (b) Suggested improved process for alkane isomerization.

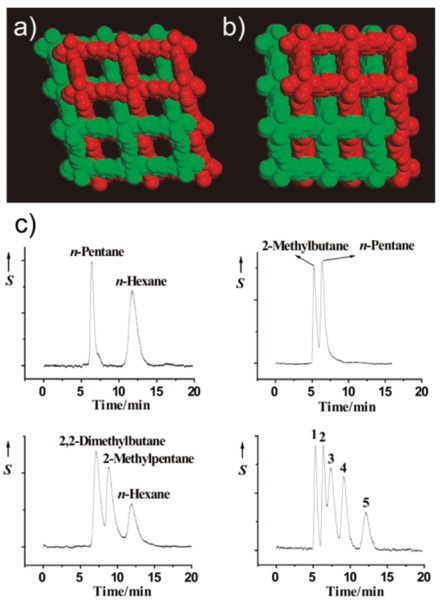

Fig. 12 (a) Space-filling representations of the structures of the open phase Zn(BDC)(4,4′-Bipy)0.5·(DMF)(H_2O)$_{0.5}$ (**MOF-508a**), which contains 1D channels of 4.0 × 4.0 Å; the disordered guest molecules in **MOF-508a** are omitted for clarity. (b) Space-filling representations of the structures of the dense phase Zn(BDC)(4,4′-Bipy)$_{0.5}$ (**MOF-508b**), viewed along the rectangular diagonal of the paddle-wheel clusters. (c) Chromatograms of alkane mixtures separated on a **MOF-508** column (bottom right: separation of an alkane mixture containing 2-methylbutane (1), *n*-pentane (2), 22DMB (3), 2MP (4), and nHEX (5)). *S* = thermal conductivity detector response.[177]

Following this study, Chen and co-workers[195] also found experimentally that hexane could kinetically separate *n*-hexane from 3-methylpentane and 2,2-dimethylbutane by fixed bed adsorption using a microporous MOF **$Zn_2(bdc)_2(dabco)$** (bdc = 1,4-benzenedicarboxylate; dabco = 1,4-diazabicyclo[2,2,2]octane). This framework contains two types of 3D intersecting pores of about 7.5 × 7.5 Å in one direction and pores of 3.8 × 4.7 Å in the other two directions. The narrow channels of 3.8 × 4.7 Å could exclusively accommodate linear *n*-hexane but block the branched isomers because of the difference in kinetic diameters of nHEX (4.3 Å), 3MP (5.0 Å) and 22DMB (6.2 Å). The efficient separation was supported by both pure components and binary vapor-phase breakthrough experiments.[195] Subsequently, this framework was further examined for the separation of a 13-component mixture of C5–C7 alkane isomers by GCMC simulations.[196] It was observed that the adsorbates with higher octane numbers are generally adsorbed weakly, with the exception of 2,3-dimethylpentane. The authors speculated that the more flexible linear alkanes might adapt to fill the available surface area more effectively.[196] Additionally, the selective adsorption of linear and monobranched hexane isomers (nHEX and 3MP) over a dibranched counterpart (22DMB) has also been observed in **$Zn_2(Hbdc)_2(dmtrz)_2$** (H_2bdc = 1,4-benzenedicarboxylate acid; Hdmtrz = 3,5-dimethyl-1*H*-1,2,4-triazole) by Zhao and co-workers.[179] Different from the 3D intersecting channel structure of $Zn_2(bdc)_2(dabco)$, $Zn_2(Hbdc)_2(dmtrz)_2$ has 1D channels of 7.0 Å × 7.0 Å in size, which is closer to the kinetic diameter of 22DMB, thus hardly adsorbed 22DMB over the whole pressure range probably because of steric effects. GC separation with this MOF was also conducted to verify its separation ability for these alkane isomers.[179]

Overall, the aforementioned examples for alkane isomer separation were controlled by the shape-selective effect, which generally depends on the subtle matching of the size and shape of the adsorbates with the adsorbent micropores. This mechanism commonly favours the adsorption of molecules with a smaller kinetic diameter, while excluding the bulkier ones. However, for **UiO-66**, a zirconium based metal–organic framework built from hexamers of eight coordinated $ZrO_6(OH)_2$ polyhedra and 1,4-benzene-dicarboxylate linkers, the elution order is completely different.[178,182,183,197] For hexane isomers, it was found that the adsorption uptake increases with the degree of branching, 2,2-dimethylbutane (22DMB) and 2,3-dimethylbutane (23DMB) being the more retained molecules. In a breakthrough column, the order of retention decreased: 22DMB > 23DMB > 3MP ≫ nHEX. The shape selectivity in contrast to the aforementioned materials might be due to the different rotational freedom of the molecules inside the small cavities, where more branched isomers are able to rotate more freely compared with the linear nHEX. This also agrees well with the results of the simulated mixture isotherms as well as the breakthrough.[198] Also, decorating the linker with different functional groups (–Br, $–NH_2$, $–NO_2$) may somewhat alter the order of elution due to the change in the pore size.[182]

Computationally, over 100 nanoporous crystalline materials, including metal–organic frameworks, have been examined for hexane and heptane isomer separation at 433 K by molecular simulations.[198] Of all the structures examined, Dubbeldam *et al.* highlighted the superior separation performance of **ZIF-77**, which is able to fractionate the alkane isomers individually according to the degree of branching. Simulations show that **ZIF-77** has a selectivity improvements of one to two orders of magnitude compared to conventional zeolites. The unique separation capability of **ZIF-77** may originate from its highly non-cylindrical structure. It has a 2D channel system with larger main channels and smaller side channels. The larger main channels could confine the linear and mono-branched molecules, while the smaller channels size-exclude the mono- and di-branched ones.[198]

Recently, Long and co-workers reported a porous iron(III) bis-pyrazolate MOF **$Fe_2(bdp)_3$** (bdp = 1,4-benzenedipyrazolate) that could efficiently separate hexane isomers into practically valuable fractions according to the degree of branching.[174] This framework has one-dimensional triangular channels with a pore width of 4.9 Å, which could accommodate all hexane isomers readily (Fig. 13). Thermodynamic analysis on the basis of single-component equilibrium adsorption isotherms at temperature from 130 to 200 °C indicates that these distinctive pore structures are able to maximize van der Waals interactions with *n*-hexane and show increasingly weaker interactions for the more branched hexanes. The linear *n*-hexane isomer has the strongest interaction with the framework because a greater fraction of its surface can interact with the triangular channel pore surface while the more compact dibranched hexane isomers have the lowest enthalpies for they are not flexible

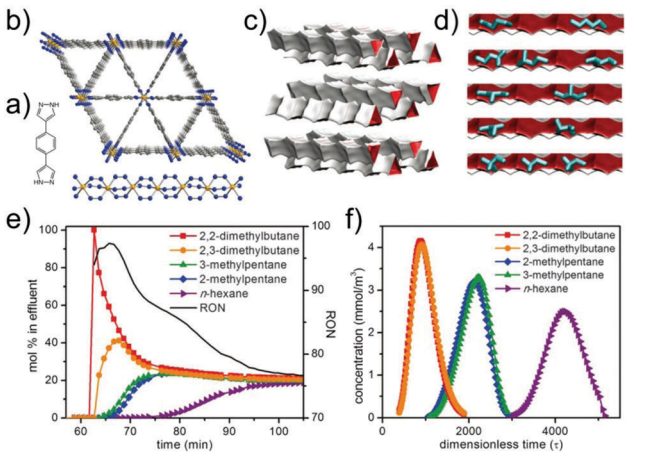

Fig. 13 (a) Chemical structure of the bridging ligand precursor H_2bdp. (b) Portions of the structure of **$Fe_2(bdp)_3$** and a perpendicular view of the one-dimensional chains of pyrazolate-bridged Fe^{III} octahedra, as determined by powder X-ray diffraction (PXRD) data (orange, blue, and gray spheres represent Fe, N, and C atoms, respectively; H atoms are omitted for clarity). (c) The van der Waals surfaces associated with the corrugated triangular channels running through the structure. (d) Snapshots of the hexane isomers within the channels of **$Fe_2(bdp)_3$** for a loading of four molecules per unit cell at 160 °C, as observed in CBMC simulations. (e) Experimental breakthrough data for the separation of an equimolar mixture of *n*-hexane isomers running through a packed bed of **$Fe_2(bdp)_3$** at 160 °C. (f) Pulse chromatography simulations calculated on the basis of single-component isotherm data.[174]

enough to maximize van der Waals interactions with the pore surfaces. Interestingly, configurational-bias Monte Carlo (CBMC) simulations calculations suggested that the size of the channels in **$Fe_2(bdp)_3$** is nearly optimal for a hexane isomer separation, narrower triangular channels cannot accommodate all five isomers, whereas wider channels do not maximize the differences in van der Waals contacts. Breakthrough experiments confirmed that this material is able to separate an equimolar mixture of hexanes into three fractions, the dibranched isomers (22DMB and 23DMB) being eluted first followed by the monobranched isomers (2MP and 3MP) and finally the linear *n*-hexane. Additionally, **$Fe_2(bdp)_3$** may be also capable of separating pentane and heptane isomers by the degree of branching.[174]

MOF materials with a channel size between the kinetic diameter of di-branched alkanes and mono-branched or linear alkanes might show distinct molecular sieving effects for their separations. Silva and co-workers recently reported a kinetically controlled molecular sieve separation between the di-branched isomer of hexane from mono-branched and linear alkanes on a flexible and ligand functionalized microporous iron(III) dicarboxylate **MIL-53(Fe)-$(CF_3)_2$**.[184] Ligand functionalization with a $-CF_3$ group narrows the pore aperture of the parent **MIL-53(Fe)**, resulting in pore diameters of 5.6 Å in large pores and 4.2 Å for narrow pores. These pore sizes were finely tuned below the kinetic diameter of 22DMB (6.2 Å) while remaining close to the dimensions of both linear nHEX (4.3 Å) and 3MP molecules (5.0 Å). The separation performance of this sorbent for an equimolar ternary mixture of nHEX/3MP/22DMB under various pressures (0.5–20 kPa) was confirmed by breakthrough experiments. Remarkably, a complete separation between 22DMB and both mono-branched 3MP and linear nHEX was achieved at 313 K and 1 kPa. The extremely weak retention of 22DMB implied that the di-branched alkane hardly enters the pore of **MIL-53(Fe)-$(CF_3)_2$**. Nevertheless, increasing the vapor pressure or temperature could lead to pore opening of this framework, as is typically observed with the flexible **MIL-53** MOFs, thus making dibranched molecules able to enter the pores more easily for a less effective separation.[184] Besides, amino functionalized **MIL-53(Al)** shows a similar adsorption hierarchy for C5–C7 isomer separation, and the separation selectivity varies from 1.7 to 3.7, and increases with the degree of branching.[190] **MIL-47**, an isostructure to **MIL-53**, also exhibits similar but somewhat lower selectivities.[191]

As a subfamily of metal–organic frameworks, ZIFs are also of particular interest for alkane isomer separation, considering they have frameworks with the same topologies as some zeolites.[175,176,181,186,199–203] The narrow pore apertures of **ZIF-8** appear to act as a molecular sieve, preventing the larger branched alkanes from diffusing into the material. Chang *et al.* reported for the first time that **ZIF-8** coated capillary columns are capable of sieving the branched alkanes from linear alkane isomers.[175] Similarly, a complete separation between the linear *n*-pentane and the branched isopentane could be realized by a molecular sieve effect.[203] It was further illustrated by means of breakthrough experiments that **ZIF-8** could act as a molecular sieve with a higher adsorption capacity to separate linear nHEX from di-branched isomer 22DMB by a kinetic mechanism, making this material a competitive alternative to zeolite 5A to improve the performance of the existing TIP processes.[176] The excellent performance of **ZIF-8** for *n*-hexane isomer separation was further supported by a recent work.[186] Silva and co-workers performed binary and ternary breakthrough experiments of nHEX/3MP/22DMB at a temperature ranging between 313 and 423 K and partial pressures up to 20 kPa. The ternary breakthrough experiments showed a complete separation of linear nHEX from the branched paraffins with a significant working capacity as high as 25 wt%. The separation is also considered kinetically driven by the gate-opening effect. Considering that the theoretical size of the accessible pore aperture (3.4 Å) is far less than the kinetic diameter of linear paraffins, it implies that the pore aperture of **ZIF-8** is also dynamically flexible during the separation.[186] The effective adsorption of 23DMB and exclusion of 22DMB observed in **ZIF-8** prove that the effective pore size of **ZIF-8** is about 5.8 Å, up to a maximum of 6.3 Å.[181] By comparison, **ZIF-76** has a large pore aperture that allows easy diffusion of all isomers. **ZIF-76** adsorbs branched alkanes more strongly than linear alkanes, thus exhibiting inverse shape selectivity.[176]

Very recently, Eddaoudi *et al.* reported a rare earth (RE) **fcu-MOF** with a suitable aperture size for the selective molecular exclusion of branched paraffins from linear paraffins.[204] The RE fcu-MOFs (**Y-fum-fcu-MOF** and **Tb-fum-fcu-MOF**) consist of two types of cages: one with an octahedral shape and the other with a tetrahedral shape (Fig. 14). Both octahedral and tetrahedral cages can be accessible through triangular windows with a diameter of approximately 4.7 Å which is slightly larger than linear paraffins (*e.g.* *n*-butane *ca.* 4.3 Å) and shorter than most mono- and dibranched paraffins (*e.g.* isobutane *ca.* 5 Å). The *n*-pentane/isopentane and *n*-butane/isobutane adsorption studies showed a complete sieving of branched paraffins from their linear isomers. It was believed that the combination of a perfect cut-off aperture size of approximately 4.7 Å and the relative rigidity allowed the RE **fcu-MOFs** to display a full molecular exclusion of branched paraffins from normal paraffins.[204]

4. Adsorptive separation of benzene over cyclohexane

Cyclohexane, as one of the key precursors in the synthesis of Nylon-6 and Nylon-66, is usually produced by the catalytic hydrogenation of benzene in the petrochemical industries.[205] Cyclohexane in the reaction product usually coexists with unreacted benzene, and separating their mixture is essential.[206–208] However, simple fractional distillation is inefficient because these molecules have similar kinetic diameters (benzene, 5.85 Å and cyclohexane, 6.0 Å) and boiling points (benzene, 80.1 °C and cyclohexane, 80.7 °C). Their separation represents a most difficult class of chemical processes. Compared to solvent extraction for benzene/cyclohexane separation, adsorption is more energy efficient and does not produce waste. To date, metal–organic frameworks have been extensively examined for

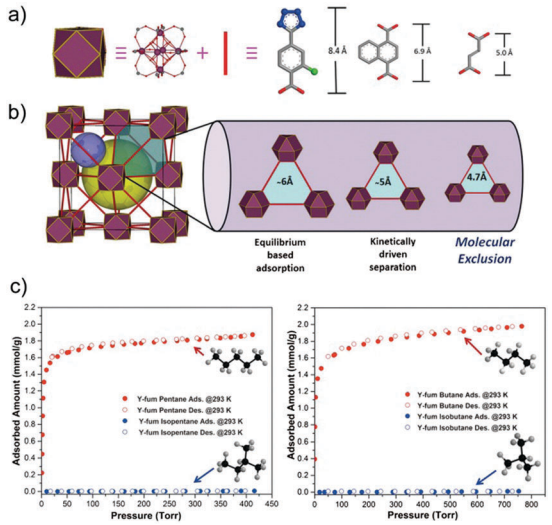

Fig. 14 (a) Schematic representation of the clusters of the **RE fcu-MOFs** including three possible organic linkers of different lengths. (b) The judicious choice of the organic linker enabled construction of the new **fcu-MOF** with the smallest aperture. (c) Single-component adsorption isotherms for *n*-pentane/isopentane (top) and *n*-butane/isobutene (bottom) on **fcu-MOF**.[204]

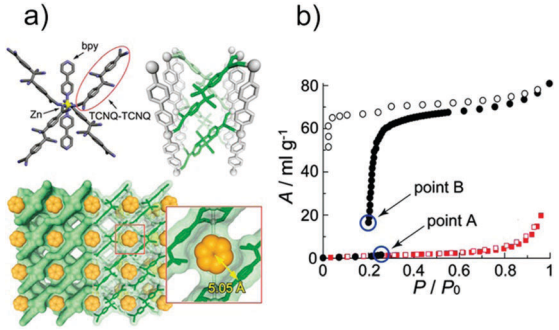

Fig. 15 (a) Coordination environment of Zn(II) ions and benzene arranged in the cage of the undulating channel of **Zn(TCNQ-TCNQ)bpy**. (b) Adsorption isotherm for benzene (top) and cyclohexane (bottom).[227]

such a separation, and some materials separated benzene from cyclohexane very effectively.[33,187,190,191,209–228]

The preferential adsorption of benzene over cyclohexane was firstly reported by Kitagawa *et al.* on **M(TCNQ-TCNQ)bpy** (M = Mn, Zn) [TCNQ = 7,7,8,8-tetracyano-*p*-quinodimethane, bpy = 4,4′-bipyridyl].[227,229] Their undulating channels delimited by the ligands comprise an alternating arrangement of two types of tube of large and small diameters. The large tube is adequate to accommodate a benzene molecule while the aperture of the small tube is not large enough for the benzene to pass through it (Fig. 15). Interestingly, when a certain number of benzene molecules accumulate on the channel surface, the strong H–π interaction between the host framework and benzene molecule triggers the structural transformation from the closed form to the open form in the sorption process. The structural flexibility further provides a more suitable space for the accommodation of benzene. In contrast, no adsorption of cyclohexane occurs even in the higher relative pressure region indicating that the gates remain closed for cyclohexane because of the absence of the H–π-type host–guest interaction.

Very similar adsorption behaviors for benzene and cyclohexane were also observed by the same group in a flexible MOF Zn(ip)(bpa) (denoted as **CID-23**, ip = isophthalate; bpa = 1,4-bis(4-pyridyl)acetylene), which has a 1D pore channel with dimensions of 5.6 × 8.6 Å. These channels allow only benzene, but not cyclohexane, to enter the channels at room temperature. After **CID-23** was exposed to the vapor of benzene/cyclohexane (1 : 1) mixtures, the ratio of the adsorbed amount of benzene over cyclohexane could reach up to 25 : 1. The very low adsorption amount of cyclohexane at near-saturated pressure resulted in high selectivity, which may be due to the structural features of flexibility and the restricted pore size of **CID-23**.[220]

Karmakar *et al.*[211] reported an amide-functionalized flexible MOF $\mathbf{Cu_2L_4(NO_3)_4}$ (L = bis(pyridinyl)-5-*tert*-butylisophthalamide) capable of preferentially adsorbing benzene over cyclohexane at room temperature. This MOF has a 1D porous framework structure, which could undergo a dynamic structural transformation into a 2D non-porous phase upon activation. Single-component adsorption isotherms of benzene at 298 K show a considerably high uptake amount but a negligible uptake amount in the case of cyclohexane. The high selectivity may originate from the much more acidic C–H proton of benzene compared to that of cyclohexane and correspondingly stronger interaction with basic amide functionality as well as π–π interaction or C–H–π interactions between benzene and the aromatic ring of the framework.[211]

Another flexible **Cu(etz)** (**MAF-2**, Hetz = 3,5-diethyl-1,2,4-triazole) can also separate benzene and cyclohexane very effectively based on the size-exclusion mechanism. **MAF-2** can readily adsorb large amounts of benzene (206 mg g^{-1}) at 298 K but only exhibits particle surface adsorption for cyclohexane. The exceptional flexible framework lattice can undergo dramatic distortions to a certain degree so that benzene can diffuse through the flexible apertures but cyclohexane cannot.[226]

The preferential adsorption of benzene over cyclohexane was also observed in an anionic framework $\mathbf{NH_4[Cu_3(OH)(4\text{-}cpz)_3]}$ (cpz = 4-carboxypyrazolato). This MOF has a 3D porous structure containing tetrahedral cages with an inner diameter of about 13 Å, which are connected through small windows of 4.5 and 8 Å in width. The NH_4^+ cations are hosted inside the large cages and are exchangeable with other cations. It was found that when this MOF was exposed to benzene/cyclohexane (1 : 1) mixtures, benzene was significantly enriched to give a ratio of 5 : 1 for benzene/cyclohexane in the adsorbed phase. Moreover, a significant enrichment of benzene over cyclohexane was observed in those MOFs after exchanging NH_4^+ with larger Et_3NH^+ or Li^+ cations, with enriched ratios of 8 : 1 and 12 : 1, respectively. This increased selectivity is most likely related to the increased bulk of Et_3NH^+ and $Li(H_2O)_4^+$ ions and correspondingly resulting in smaller pores in the MOF.[230] Additionally, a trinuclear cluster-based microporous MOF $\mathbf{Ni_3(OH)(Ina)_3(bdc)_{1.5}}$ (Ina = isonicotinate and bdc = 1,4-benzenedicarboxylate) has been observed in which the amount of adsorbed benzene (22.60 wt%) is much

higher than that of cyclohexane (1.40 wt%). The higher uptake of benzene may be due to the π–π interactions between the benzene guest and the phenyl ring of the framework.[218] Such a favourable role of π–π interactions between benzene and the frameworks has also been explored to design MOFs with improved separation selectivity of benzene over cyclohexane.[210,212] The strategy of simultaneous incorporation of both electron-rich and electron-deficient functionalities in covalent–organic frameworks has also been utilized to address the separation of benzene from cyclohexane. A porous covalently linked triazine based framework **CTF-IP10**, built from a tripodal cyano-based monomer, shows a selective uptake of π-electron rich benzene up to 12.43 mmol g^{-1} and IAST selectivity for equimolar benzene/cyclohexane mixtures is in excess of about 50 owing to the stacking interaction between electron-rich benzene and electron deficiency of the triazine rings.[231]

In contrast to the aliphatic cyclohexane, the benzene molecule is a π-cloud entity, therefore it is a potential strategy to selectively adsorb benzene by π-complexation triggered facile Lewis acid–base interactions between the open metal sites of MOF and benzene. Recently, Mukherjee *et al.* reported for the first time exploiting Lewis acid–base interactions between coordinatively unsaturated sites of **M-MOF-74** (M = Mg, Mn, Fe, Co, Ni, Cu, Zn) series of frameworks and benzene to realize efficient selective benzene sorption over cyclohexane. IAST calculations show that the selectivity of **Mn-MOF-74** is exceedingly high in excess of 10^5 for equimolar cyclohexane/benzene mixtures. These high selectivity values propel this series of MOFs as top-notch cyclohexane/benzene separating materials.[232]

5. Adsorptive separation of aromatic C8 isomers

The separation of mixed C8 alkylaromatic compounds is of great interest in the petrochemical industry as xylene isomers and ethylbenzene (EB) are important chemical raw materials in several industrial processes. *ortho*-Xylene (OX) is used to produce phthalic anhydride, which is used as a plasticizer. *meta*-Xylene (MX) is used to produce isophthalic acid, which is gaining broader acceptance in polyethylene terephthalate (PET) resin blends, or can be isomerized into the other C8 isomers. *para*-Xylene (PX) is the isomer with the broadest commercial use since it is used in the manufacture of terephthalic acid, which is the basis for PET production. EB is finally used to dehydrogenate styrene for polystyrene production. However, these C8 alkylaromatics boil so closely together that conventional distillation is not feasible except for the removal of OX which has a boiling point at least 5 °C above the others (Table 2). Nevertheless, an enormous column of about 150–200 plates and a high reflux ratio are necessary.[233]

Basically, the separation of high-purity PX from the mixed C8 isomers is industrially performed by two main processes: crystallization and adsorption. Comparatively, adsorption processes are preferred for their larger production rate, lower cost and significantly higher recovery of PX. There are three main industrial processes for PX separation from mixed xylenes: UOP's Parex, Toray's Aromax, and IFP's Eluxyl.[234] These processes rely on a simulated moving bed (SMB) technology, which allows a continuous separation using faujasite zeolites exchanged with cations such as Na^+, K^+, and Ba^{2+}.[235]

Table 2 Physical properties of xylene isomers

	PX	MX	OX	EB
Boiling point (°C)	138.38	139.19	144.44	136.21
Kinetic diameter (Å)	5.8	6.8	6.8	5.8
Dipole moment (D)	0.1	0.37	0.64	0.59
Polarizability, σ (cm^3)	137	142	141	142

As the PX content in the xylene feedstock is in the range of 17–24%, the ideal adsorbents should preferentially bind PX in light of a higher productivity. PX has the lowest boiling point and the lowest moment (Table 2) among xylenes, finding *para*-selective adsorbents is however challenging. Although the industrially used adsorbents (BaX and KBaY) are *para*-selective on the basis of the hierarchy of adsorption strengths dictated by molecular packing or entropic effects, the selectivity of PX over MX along with the uptake of PX is nevertheless low. The improvement of these processes continues to bean interesting industrial challenge.

As MOFs possess a higher degree of tailorability because of the almost infinite number of possible metal–ligand combinations, they offer great potential for the discovery of MOFs that have higher selectivity and uptake to adsorb PX instead of BaX zeolite in the SMB and thus to improve these separations. Industrially, since xylene separation is operated in the liquid phase in the SMB unit, the pores of the adsorbent materials are practically saturated with guest molecules. Under liquid-phase conditions, the hierarchy of adsorption strengths is dictated by molecular packing or entropy effects. The binding energies of guest molecules with the framework walls or non-framework cations do not solely determine the separation performance.[188] In a search for MOF materials with PX isomer preferences, only a few MOFs have shown interesting features in the selective adsorption of PX. Early work on metal–organic frameworks hinted at their ability to separate C8 alkylaromatics. For example, a zinc 2,6-naphthalene dicarboxylate framework $[\mathbf{Zn_2(ndc)_2(DMF)_2}]$ (ndc = 2,6-naphthalene dicarboxylate), isostructural with **MOF-105**, is found to include PX with high selectivity from mixtures of xylene isomers during the crystallization of the MOF.[236] Although Vos and co-workers[237] claimed that the vanadium(IV) terephthalate **MIL-47** is the first example of a MOF used as a highly *para*-selective adsorbent for the liquid-phase separation of PX *versus* MX and PX *versus* EB, however, **MIL-47** fails to discriminate between PX and OX. Actually, **MIL-47** has been proven to be an *ortho*-selective material by the follow-up investigations, for either vapor-phase or liquid phase adsorption.[237–241] Indeed, the monoclinic MOF, $\mathbf{Zn_3(bdc)_3(H_2O)_3(DMF)_4}$ (bdc = 1,4-benzenedicarboxylate), might be the first example of an material capable of a preferable adsorption of PX over other isomers. Vapor-phase breakthrough experiments of quaternary mixtures of PX/MX/OX/EB over this material show that the order of adsorption is

EB < OX ≈ MX < PX, agreeing with the elution order in pulse GC. The monoclinic MOF gave an average selectivity of 2.52, 5.17, and 4.55 for the separation of MX/PX, EB/PX, and OX/PX binary mixtures, respectively. The authors claim that the preferable adsorption of PX originated from the faster diffusion rates into the material relative to other isomers, which is quite surprising since the critical diameters of EB and PX are very similar. For comparison, another Zn-terephthalate **MOF-5** was also examined and found to be able to experimentally separate EB from other xylene isomers in a breakthrough column at 523 K.[242]

Another *para*-selective material is **JUC-77**, In(OH)(oba)(H_2oba = 4,4′-oxybis(benzoic acid)), which has rhombus-shaped channels running in two perpendicular directions. The rhombic 1D-channels have the diagonal sizes of 10.8 × 7.3 Å, which are close to the dimensions of the xylene isomers. The channels may act as molecular sieves for the xylene isomers. PX that has the smallest width can enter into the rhombic channel easily, while MX and OX are sterically excluded. Unfortunately, the adsorption of EB was not investigated.[243] Huang *et al.* also reported a *para*-selective Zn-MOF featuring hexagonal nanochannels with a diameter of approximately 14.8 Å. The preferable adsorption of PX over MX and OX both in liquid and vapor phases were confirmed by H^1 NMR characterization as well as static adsorption experiment.[244]

In search of *para*-selective MOFs, a more efficient approach would be computational screening of the candidate MOF structures with cages or windows in a range comparable with the kinetic diameters of xylene isomers. Based on this strategy, three isostructural metal–organic frameworks, **MIL-125(Ti)** ($[Ti_8O_8(OH)_4(BDC)_6]$), **MIL-125(Ti)-NH_2** ($[Ti_8O_8(OH)_4(BDC\text{-}NH_2)_6]$), and **CAU-1(Al)-$NH_2$** ($[Al_8(OH)_4\text{-}(OCH_3)_8(BDC\text{-}NH_2)_6]$) (BDC = 1,4-benzenedicarboxylate), capable of selectively isolating PX from a mixture of xylenes were proposed.[245] The *para* selectivity may originate from their unique structure containing two types of cages. As exemplified by **MIL-125(Ti)-NH_2**, the quasi-cubic tetragonal structure is built from cyclic octamers of edge- and corner-sharing TiO_5(OH) octahedra that are connected by 2-aminoterephthalate linkers. Each octamer is surrounded by 12 secondary building unit neighbors, resulting in a 3D structure that contains two types of cages. The large octahedral cages have a 1.25 nm accessible diameter, while the smaller tetrahedral cages may have an approximate diameter of 0.61 nm. The two types of cages are connected through triangular cage windows with an aperture size in the range 0.5–0.7 nm. Microcalorimetric experiments confirmed the preferential interaction of the material with PX, and molecular simulations reveals that both OX and MX are adsorbed in a rather disordered way in the centre of the octahedral cages, in which PX manages to pack more efficiently and maximize adsorbate–adsorbate as well as adsorbate–framework interactions. Breakthrough experiments for equimolar binary solutions of xylene isomers in heptane also confirm the results of the simulations. Average separation factors of 2.2 for PX *versus* OX and 3 for the important couple PX *versus* MX were obtained. Remarkably, **MIL-125(Ti)-NH_2** also prefers PX over EB, with a separation factor of 1.6 calculated from a breakthrough experiment, further proving that molecular sieving is not the only mechanism determining the PX selectivity but that the shape of the molecules has a large influence as well on the preferential adsorption of PX in the octahedral cages.[245]

In a follow-up study, the effect of EB on the PX selectivity of **MIL-125(Ti)-NH_2** was investigated with ternary and quaternary breakthrough experiments in the liquid phase using *n*-heptane as an eluent.[246] These experiments confirmed that **MIL-125(Ti)-NH_2** is a *para*-selective material as PX is the most retained isomer, even in the presence of MX and OX isomers. However, the *para*-selectivity decreased when the concentration of xylene isomers increased. The presence of EB in the feed strongly impacts the selectivity of PX/EB, dropping from 1.4 at low concentrations to even inversed selectivity of 0.8 at higher EB concentrations. These observations showed that the sieving effect is more favourable to the PX than to EB, and that **MIL-125(Ti)-NH_2** becomes EB selective at high feed concentrations due to more efficient stacking of EB molecules in the octahedral cages of the structure.[246] Similar phenomena were also observed in the parent **MIL-125(Ti)**.[247]

A conceptual strategy based on the differences in the stacking efficiencies of C8 aromatics within the MOF channels was recently adopted by Torres-Knoop and co-workers, with the goal of finding MOFs that selectively adsorb PX.[248] They used CBMC simulations to systematically screen a wide variety of MOF candidates, including **MAF-X8**, **Co(BDP)**, **MIL-125(Ti)**, **MIL-125(Ti)-NH_2**, and **JUC-77**, that are capable of the desired selectivity towards PX. Among these MOFs, transient breakthrough simulations of quaternary mixtures of PX/MX/OX/EB confirm that **MAF-X8** shows the best *para* selectivity, and is comparable to that of zeolite BaX, which is currently used in industry. **MAF-X8** outperformed the other MOFs because the channel dimensions and geometry allow more efficient and commensurate stacking of PX molecules (Fig. 16b). Moreover, CBMC simulations revealed that the PX adsorption capacity of **MAF-X8** might be significantly higher than BaX.

5.1 Selective adsorption based on breathing effects

Apart from the above-mentioned rigid MOFs, flexible MOFs can also perform the separation of C8 isomers, and undergo ''breathing''-type structural changes when sorbing C8 aromatics. Recently, Warren *et al.*[249] described a flexible MOF **[Ce(htcpb)·$(EtOH)_{0.28}(H_2O)_{2.75}$]** ($H_4$tcpb = tetradentate carboxylic acid) that takes up PX highly selectively over MX. The authors demonstrated that the favorable and unfavorable channel restructuring for PX and MX, respectively, amplifies the MOF's selectivity in separations of the two isomers. The MOF has two types of one-dimensional channels (Fig. 17). Notably, the channels can undergo guest-driven structural relaxation involving geometric changes around the metal (cerium) ions and rotation of a benzene ring in the organic linkers, leading to high *para*-selectivity by differentiating the response flexibility between the two molecules. The restructuring around the preferred PX enhances an energetically favorable docking through localized expansion and contraction, while the flexibility needed to accommodate MX mismatches between a larger distortion of the host and MX positional disorder. The adsorption selectivity of PX over

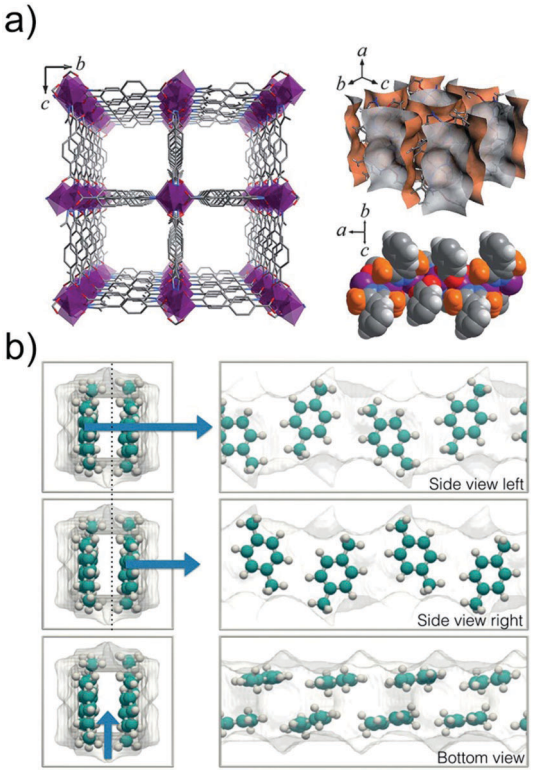

Fig. 16 (a) Perspective view of the framework structure and the pore surface of **MAF-X8** as well as its side view of the Zn-carboxylate chain in the space-filling mode (methyl groups are highlighted in orange). (b) Stacking of *p*-xylene in the **MAF-X8** structure.[248]

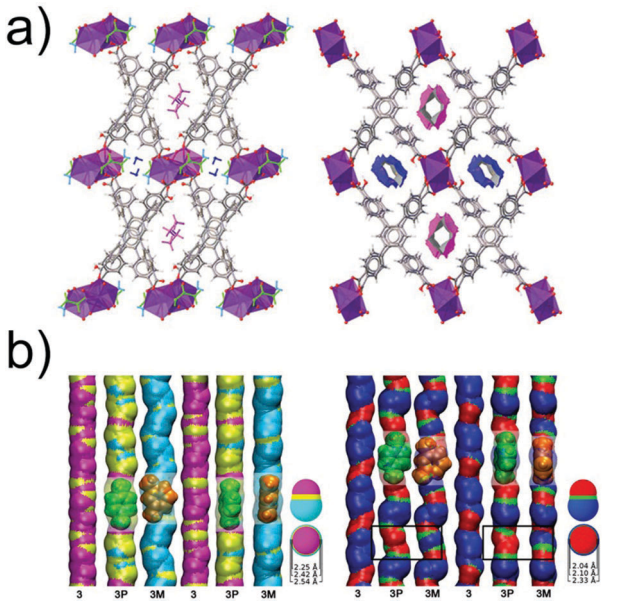

Fig. 17 (a) Crystal structures of as-synthesized (left) and desolvated MOF **Ce(Htcpb)**. (b) *para*-Xylene and *meta*-xylene loaded channel surfaces for the two types of channels in **Ce(Htcpb)**.[249]

MX of 4.5 was determined by GC measurements, and the selectivities for PX over OX and EB of 5.6 and 2.4, respectively, are also considerably high.[249]

In a recent paper, Mukherjee *et al.*[250] have reported another flexible MOF **[$Zn_4O(L)_3$]**, (L = 4,4′-((4-(*tert*-butyl)-1,2-phenylene)-bis(oxy))dibenzoate), also denoted as **DynaMOF-100**, which is capable of selectively adsorbing PX over its congener C8 alkyl-aromatic isomers. The ligand used bears two ether linkages as its flexible nodes. The resultant MOF shows a high degree of framework flexibility owing to the ether linkages actually functioning as the adjustable nodes. The vapor-phase isotherm at 298 K shows that the adsorption uptake for the PX was found to be 64 mL g^{-1}, and the corresponding uptake amounts for the *m*- and *o*-isomers were surprisingly much lower, 5 mL g^{-1} and 1.15 mL g^{-1} respectively (Fig. 18). A very marginal uptake for EB of only 9.4 mL g^{-1} was recorded. Remarkably, IAST calculations of separation selectivities in favor of PX for **DynaMOF-100** was estimated to exceed 100, significantly higher than that for BaX and **MAF-X8**.[251] This clear preference for PX over the other isomers might originate from the structural transformations occurring on the interplay of host–guest interactions. Further experimental work on breakthroughs, and stability tests are required in order to demonstrate the efficacy of **DynaMOF-100** for the replacement of BaX in the SMB process.[250]

To replace the energy-demanding xylene splitter and OX distillation column in an existing state-of-the-art aromatics plant, highly OX-selective adsorbents would also be desired. The most extensively investigated MOFs for separating C8 aromatic hydrocarbons are the terephthalate-based structures with one-dimensional lozenge-shaped channels, *e.g.* **MIL-53(Al).**[233,252–264] One of the striking characteristics of **MIL-53(Al)** is the framework flexibility, featuring the stepwise adsorption caused by guest-induced framework transitions. Finsy *et al.* studied the framework breathing in the vapor-phase adsorption and separation of xylenes with **MIL-53(Al).**[253] The adsorption and desorption isotherms of the pure components at 110 °C show two well-defined steps and hysteresis, corresponding to the opening or breathing of the framework, as induced by the presence of the adsorbed molecules. At low pressure below the "pore-opening" pressure, **MIL-53** shows no preference for any isomer, while at pressures high enough to induce pore-opening the space is sufficiently large for the xylene isomers to be accommodated in pairs along the length of the pores. The framework flexibility induced by the xylene loading can also be detected by monitoring the evolution of the dynamics of fragments (terephthalate phenylenes) of the MOF with temperature by means of ^2H solid state NMR.[263]

The structure flexibility of **MIL-53(Al)** creates a separation environment that is highly dependent on total pressure, as at 110 °C the separation is very poor at 0.9 mbar but significantly improved at 0.056 bar.[253] By comparing the desorption temperature by thermogravimetric analysis, it can be found that the adsorption strength between isomers and the framework in **MIL-53(Al)** follows the order of OX > MX > PX > EB,[262] which is consistent with the elution order obtained on a column packed with **MIL-53(Al)** crystallites by means of chromatographic separation.[252] The feasibility of separating *ortho*-xylene from the other isomers was further validated by competitive batch

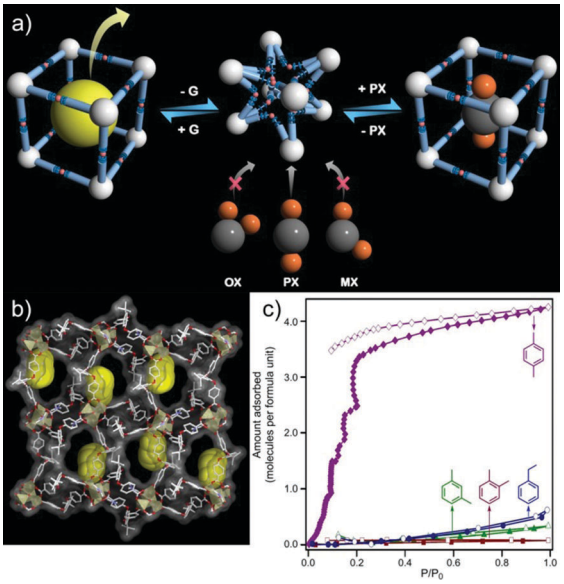

Fig. 18 (a) Schematic representation of the framework flexibility with selective guest-accommodation. (b) Overall structure of the resolvated phase showing free PX molecules in the channels (PX molecules are shown in the spacefilling model for clarity). (c) Solvent sorption isotherms at 298 K for three of the xylene isomers along with isomeric ethylbenzene.[250]

adsorption experiments as well as breakthrough experiments. As evidenced by Rietveld refinements of PXRD data sets, a stronger deformation of the channels of **MIL-53** adsorbing OX was observed compared to the effect of adsorption of the *meta*- or *para*-isomer. It was believed that the channel deformation is dependent on the strength of interactions between methyl groups and the framework. The molecular geometry of OX allows for the interaction of both methyl groups with the carboxylate groups of the framework, while MX and PX molecules can only interact with the carboxylate groups *via* one methyl group simultaneously.[252,262]

Inspired by the strong *ortho*-selectivity of **MIL-53(Al)**, it makes sense to find an appropriate eluent for using this material under industrial process conditions. It was found that the *ortho*-selectivity could be affected by the choice of the eluent or mobile phases for the xylene isomer separation in the liquid phase.[255,261] Using *n*-heptane as an eluent could obtain higher selectivity when compared to iso-octane and *n*-hexane. Breakthrough experiments with the three different solvents further confirmed the *ortho*-selectivity of the material and demonstrated that the eluent plays an important role in xylene separations.[255] The optimal solvent system was further adopted by Rodrigues *et al.* for measuring the adsorption equilibrium data on the pelletized form of **MIL-53(Al)**. On the basis of these equilibrium data, the SMB simulation reveals that **MIL-53(Al)** shows great potential for the complete separation of OX from the other xylene isomers.[233]

Excellent C8 alkylaromatics separation in **MIL-53** is not limited to the aluminum isostructure. In a variety of experiments, xylene isomers have been found to behave differently in the pores of **MIL-53(Fe)**.[259,264] Compared to **MIL-53(Al)**, which shows poor selectivity between *para* and *meta* isomers,[237,252,256] **MIL-53(Fe)** is able to separate both isomers in breakthrough experiments.[259] Pulse chromatography validated that baseline separation of xylene isomers could be achieved on the **MIL-53(Fe)** packed column in the reverse-phase mode, which even exhibited better separation performance than the **MIL-53(Al,Cr)** packed columns, but shows MX-selectivity.[264] In addition to **MIL-53(Fe)**, a gallium-based **MIL-53** analogue based on *trans*-1,4-cyclohexanedicarboxylic acid instead of terephthalate also shows a high degree of framework flexibility towards OX,[265] while a Mn-based **MIL-53** analogue with pyridine *N*-oxides as μ_2-O substitutes shows potential for the separation of C6, C7, and C8 aromatics in the liquid phase.[266]

Another kind of aluminium-based flexible MOF, structurally related to **MIL-53**, was **CAU-13** ([Al(OH)(*trans*-CDC)] (*trans*-H_2CDC = *trans*-1,4-cyclohexanedicarboxylic acid) reported by Niekiel *et al.*[267] During the synthesis of CAU-13 *via* solvothermal reaction, the flexible aliphatic linker *trans*-H_2CDC is able to undergo conformational changes, leading to an equilibrium between the *e*,*e* and *a*,*a* conformers (1 : 1), which are both present in the structure of **CAU-13**. Structure determinations of **CAU-13** loaded with the xylene isomers reveal a remarkable breathing effect. The adsorption of xylene isomers induces a larger pore opening (11 Å) than that in the thermal activation of **CAU-13** (9.7 Å) by a conformational change of the flexible aliphatic linker molecules from the *a*,*a* conformation to the *e*,*e* conformation. Liquid-phase adsorptions of the xylene mixture show slight selectivities of 1.7 for the separation of OX and PX and 2.1 for the separation of OX and MX.[267]

MIL-47(V), also an important member of the MIL family, which is isostructural to **MIL-53(Al)**, has also been studied extensively for C8 alkyaromatic separations.[237–241,252,257,260,268–270] In contrast to the flexible properties of **MIL-53(Al)**, the absence of μ_2-OH groups in **MIL-47(V)** essentially leads to a rigid framework regardless of the nature of the stimulus. Vos and co-workers demonstrated the first example using **MIL-47(V)** for the separation of xylene isomers. Compared to **MIL-53(Al)**, **MIL-47** is only marginally effective at discriminating between OX and PX, but quite remarkably preferred PX over MX.[237] Breakthrough experiments with diluted xylene isomer mixtures in hexane using a MIL-47 packed column gave average selectivities of 2.5 for the separation of PX and MX and 7.6 for the separation of PX and EB. Rietveld refinements of the XRD patterns of **MIL-47** samples saturated with each of the isomers in the liquid phase shows that the selectivity in xylene isomer adsorption arises from the differences in molecular arrangements of the adsorbed molecules in the pores. Given the very limited available space and freedom in the 1D micropores of **MIL-47**, molecular packing effects become critical under liquid-phase conditions.[237,269] In the follow-up work, pore-filling dependent selectivity effects in the vapor-phase separation of xylene isomers by **MIL-47** were analyzed by performing breakthrough adsorption experiments. Also, the adsorption selectivity was found to increase with an increasing degree of pore filling or partial pressure, as observed by grand canonical Monte Carlo simulations.[271] Similar to findings in the liquid phase, the separation at a high degree of pore filling in the vapor phase

is a result of differences in the packing mode of the C8 isomers in the pores of **MIL-47**, which has already been supported experimentally by ^{2}H solid-state NMR.[238,269] The molecular packing of xylene isomers inside the confines of the **MIL-47** pores was also demonstrated by high quality DFT calculations. As the interaction energies are very similar for all isomers, entropic effects might be mainly responsible for the adsorption selectivity.[241,260]

5.2 Selective adsorption based on shape-selective effects

The zirconium terephthalate MOF **UiO-66** may be another most promising material outside of the MIL family for separations of xylene isomers.[178,272–278] Extensive studies have confirmed that **UiO-66** is also a highly *ortho*-selective material by molecular simulations and pulse chromatography as well as breakthrough experiments, although the crucial separation between the *para* and *meta* isomers is only modest.[272,275] **UiO-66**, built from zirconium oxoclusters $Zr_6O_4(OH)_4$ and 1,4-benzenedicarboxylate (BDC or terephthalate), exhibits a cubic 3D structure with two types of microporous octahedral (~11 Å) and tetrahedral cages (~8 Å) that are accessible through microporous windows of around 5–7 Å.[279] The critical kinetic diameters of EB, PX, MX and OX are 6.7, 6.7, 7.1 and 7.4 Å, respectively, which is comparable with the size of the smaller cage. Multicomponent adsorption of xylene isomers in **UiO-66** was experimentally studied by means of quaternary breakthrough curves of an equimolar mixture at a total pressure of 1 and 10 kPa, and temperatures of 398 and 423 K by Bárcia *et al.*[178] It was observed that the adsorption of the bulkier OX is favored over the other isomers and presents a selectivity pattern that is reversed from that of the xylenes' molecular dimension,[178] which agrees well with the elution order of xylene isomers from a silica–UiO-66 composite packed column using a hexane/dichloromethane mixture as an eluent.[276,277] The reverse shape selectivity may be dictated by the rotational freedom of the adsorbed molecules inside the smaller cavity of **UiO-66** as the van der Waals volumes of EB, PX, MX and OX are 120.20, 120.13, 120.04 and 119.91 nm^3, respectively.[178] In the follow-up work, the powder or shaped **UiO-66** as agglomerates and tablets were evaluated for the selective adsorption and separation of xylene isomers in the liquid phase. Pulse experiments performed at 313 K, using *n*-heptane as the eluent, revealed the OX preference of this material, which was further confirmed by binary and multicomponent breakthrough experiments, resulting in selectivities at 313 K of 1.8 and 2.4 with regard to MX and PX, respectively.[273] A preferential adsorption of OX over the other xylene isomers is also found on other **UiO-66** functionalized analogues.[274]

Another MOF exhibiting shape-selective adsorption for the separation of aromatic C8 hydrocarbons is **CD-MOFs**, which are body-centered cubic and are composed of six γ-cyclodextrin (γ-CD) units coordinated by the alkali metal cations to form the transverse channels (Fig. 19).[280] Given that CD-based chromatographic packing has been widely used for enantiomer separations, in the same manner, the shape and topology of the hydrophobic cavities of **CD-MOF** frameworks could be utilized for isomer

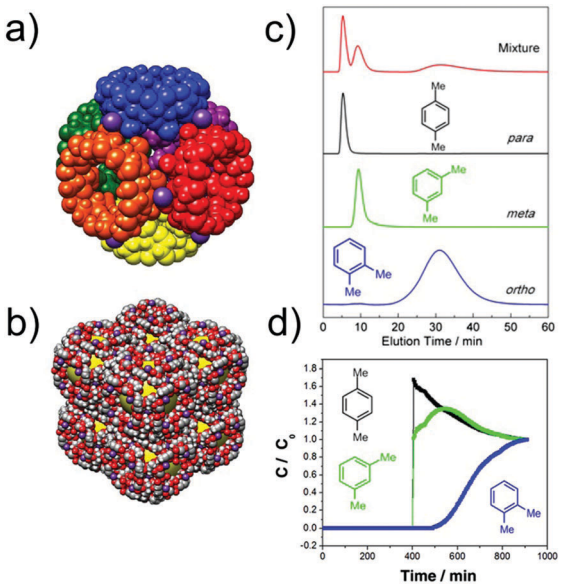

Fig. 19 (a) The cuboidal topology of **CD-MOF**, in which each γ-CD is represented as a space-filling display. (b) A space-filling representation of **CD-MOF**. (c) Liquid-phase chromatographic separations of xylene mixtures using hexane as the mobile phase and **CD-MOF** as the stationary phase. (d) Vapor-phase breakthrough experiments on **CD-MOF**.[280]

separations. Liquid-phase chromatographic measurements using *n*-hexane as the mobile phase indicate that **CD-MOF** exhibited a complete separation of OX from both PX and MX, but a partial separation of PX and MX. The selectivity for OX over PX is as high as 16.4 and the factor for MX over PX of is 3.44. Vapor-phase xylene breakthrough experiments on **CD-MOF** also demonstrated its separation performance and *ortho*-selectivity. Computational simulations revealed that *ortho*-selectivity arose from a highly efficient π–π stacking of OX within the framework and favourable adsorbent–adsorbate interactions.

5.3 Selective adsorption based on gate-opening effects/molecular sieving effects

Window flexibility also plays an important role in the adsorption of xylene isomers on zeolitic imidazolate frameworks.[199,281–284] This window flexibility opens up new opportunities for ZIFs as potential materials with unique separation capabilities. For example, Peralta *et al.*[281] reported for the first time that **ZIF-8** that could accommodate PX, based on ^{1}H NMR analysis and XRD characterization studies, although the nominal aperture size (~3.4 Å) of **ZIF-8** should not even allow the xylene isomers to enter into the pore system because of the larger kinetic diameters of xylenes. This surprising flexibility might be attributed to the transitory opening of the aperture, which behaves like a saloon door that opens when the molecule passes and closes again when they have entered the cage. The deformed pore aperture was estimated to be 6.4 Å, which is close to the kinetic diameter of PX.[281] When the xylene molecules pass through the pore aperture of six-membered rings, the initial conformation of **ZIF-8** is distorted, *i.e.* the imidazolate linkers are tilted in order to favor the diffusion of xylenes through the

window. For molecules larger than 5.8 Å, the diffusion of xylenes into **ZIF-8** becomes extraordinarily slow.[284] The strong dispersion of the breakthrough fronts and the absence of a roll-up in the breakthrough curve of the more weakly adsorbed species indicates that the separation of xylene isomers is manipulated by a kinetic separation mechanism.[282] It has been observed that **ZIF-8** shows a diffusion selectivity of 4.0 and 2.4 for PX/OX and PX/MX, respectively.[284] The breakthrough separation of a quaternary mixture of PX/MX/OX/EB shows an increasing elution order of OX < MX < EB < PX, which is entirely coherent with a separation mechanism based on molecular sieving. Additionally, another zeolitic imidazolate framework **ZIF-68** also shows a diffusion selectivity of 3.8 (2.2) for PX/OX (PX/MX) because of a certain degree of structural flexibility.[201]

Experimentally, **$Zn_2(bdc)_2(dabco)$** has been shown to separate hexane isomers, and it also binds C8 alkylaromatics preferentially, with the Henry's constants following the order OX > MX > EB > PX. The theoretical **$Zn_2(bdc)_2(dabco)$** selectivity for OX over the other C8 aromatics lies between 1.4 and 1.9 at temperatures as high as 448 K.[285] The quaternary vapor-phase breakthrough experiments show feasible separation of OX from other C8 aromatics with *ortho*-selectivity up to 1.88 at 448 K.[286]

6. Separation of styrene and ethylbenzene

Styrene (ST) is the most industrially important aromatic monomer used to produce many commercial polymers and copolymers owing to the high reactivity of its vinyl group. Ethylbenzene (EB), produced from the alkylation of benzene with ethylene, is the feedstock for catalytic dehydrogenation to form ST. The dehydrogenation of EB into ST accounts for about 60–80% conversion, and the reaction product still contains unreacted EB. Because of their close boiling points (ST (bp 418.3 K) and EB (bp 409.3 K)), ST and EB are currently separated by highly energy-intensive vacuum distillation.[287,288]

Yan *et al.* reported the first example of **MOF-199** as the stationary phase in gas chromatography for ST/EB separation though along with other benzene homologues.[289] Excellent separation of ST and EB was confirmed using the commercial **$Cu_3(btc)_2$** (Basolite C 300) as the stationary phase in HPLC.[290] Resolution for this separation can be significantly improved on silica–**$Cu_3(btc)_2$** composites in HPLC owing to the monodisperse silica supporter, giving the resolution factor of 7.9.[291] Batch adsorption and breakthrough experiments have also been performed to elucidate the capacity of **$Cu_3(btc)_2$** to separate ST and EB.[292]

Similarly, an **MIL-101(Cr)** packed column offered high-resolution separation of ST and EB. Stronger retention for ST than EB on the packed column may arise from the π–π interaction between the styrene and aromatic framework walls and the coordinative interaction of styrene with the unsaturated metal sites.[293] The same elution order of EB and ST agreed with that observed on **$Cu_3(btc)_2$** with the unsaturated metal sites as well.[290,291]

Apart from the remarkable performance for the separation of xylene isomers, **MIL-47** is also capable of separating styrene (ST) and ethylbenzene (EB).[268,294] Vos and co-workers first reported that ST could be preferentially adsorbed by both **MIL-47** and **MIL-53(Al)**.[268] Although both frameworks are structural analogues, the adsorption mechanisms are quite different because of significant characteristics of structure flexibility. For the rigid **MIL-47**, ST is packed inside the channels in a unique pairwise fashion, also known as a sort of entropic nature, while the preferential adsorption of ST in **MIL-53(Al)** is related to the difference in enthalpy of adsorption that depends on the degrees of framework distortion. **MIL-47** adsorbed a similar amount of both compounds with **MIL-53(Al)** and **$Cu_3(btc)_2$**, but both batch adsorption and breakthrough experiments revealed the selectivity of ST over EB on **MIL-47** was superior to **MIL-53(Al)** and **$Cu_3(btc)_2$**.[268,292,294]

Ghosh and co-workers[270] investigated the separation of EB and ST on the structurally flexible **DynaMOF-100** featuring a highly dynamic adaptable framework. The structural transformation can be triggered on inclusion of ST within the framework. The selectivity of ST over EB may arise from the better molecular packing of the planar ST molecules within the MOF channels. IAST calculations for the separation of EB/ST mixtures showed a significant superiority of **DynaMOF-100**, with a selectivity of approximately 1 to 2 orders magnitude higher than that of **MIL-47(V)** and **MIL-53(Al)**.[270]

Baseline separations of EB and ST were also achieved on an aforementioned **CD-MOF-1** column in HPLC with EB eluting from the column before ST, giving a selectivity of 1.75. Quantum mechanical calculations revealed that EB prefers to adopt a relative orientation such that its aromatic ring lies almost perpendicular to the C8 axis of γ-CD whereas ST prefers to orient itself almost parallel to the C8 axis and closer to the inner wall of the γ-CD ring.[295] In contrast to most MOFs, baseline separation was observed on the hydrophobic **MAF-6** column in gas chromatography with EB more strongly retained than ST. This uncommon phenomenon may arise from the stronger van der Waals interaction between the MOF and the more lipophilic EB.[187]

7. Separation of halogenated aromatics

Halogenated aromatic hydrocarbons, particularly chlorinated aromatics, are important starting materials and additives in the production of insecticides, fungicides, herbicides and so forth. Halogenated aromatics are prepared industrially by the reaction of liquid benzene with gaseous chlorine. Generally, mixtures of positional isomers and compounds with varying degrees of chlorination are obtained in the reaction products.[296] They are desirable to be separated into individual isomers. Investigations into the separation of chlorinated aromatics on the MOFs are mostly performed by chromatography.[180,261,264,293,297,298]

Alaerts *et al.* reported the liquid-phase adsorptive separation of *meta*-dichlorobenzene and *para*-dichlorobenzene on **MIL-47**, which prefers to adsorb *para*-dichlorobenzene.[240] Compared to **MIL-47**, the isostructural **MIL-53(Al)** shows much better performance for HPLC separation of a mixture of *ortho*-, *meta*- and *para*-dichlorobenzene with the same elution order.[297] HPLC separation of these positional isomers on **MIL-53(Al)** and **MIL-101(Cr)** columns can be significantly improved by changing the composition of the binary mobile phase.[261,293] Apparently, **MIL-53(Fe)** is able to discriminate *ortho* and *para* isomers of dichlorobenzene under reverse-phase HPLC.[264] Baseline resolution was achieved on a **MOF-CJ3** coated capillary in GC for the separation of these chlorinated aromatics.[180] Nevertheless, the mechanisms for the separations of chlorinated aromatics on these MOFs were still not clear though they might be entropically favourable.

Considering the fact that the unique separation possibilities are feasible with triangular channel geometry,[174,299] Torres-Knoop and co-workers[300] demonstrated an example of the separation of trichlorobenzene (TCB) isomers within a $\mathbf{Fe_2(BDP)_3}$ variant by means of configurational-bias continuous fractional component Monte Carlo simulations. Simulation snapshots revealed that only 1,3,5-TCB has the right size to reorient into optimum face-to-face stacking within the channels of the $\mathbf{Fe_2(BDP)_3}$ variant. The simulated isotherms indicate that 1,3,5-TCB can be selectively separated from its 1,2,4-TCB and 1,2,3-TCB isomers, especially under saturation conditions (Fig. 20).

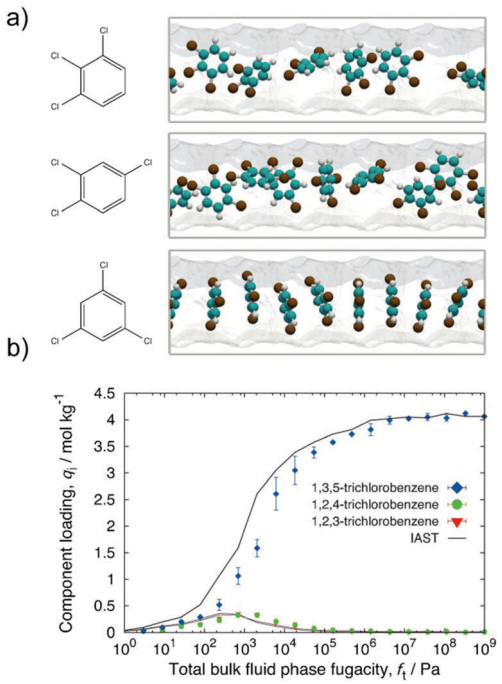

Fig. 20 (a) Snapshots of trichlorobenzene isomers in the $\mathbf{Fe_2(BDP)_3}$ variant, and only 1,3,5-trichlorobenzene is able to reorient into a pile configuration. (b) Mixture isotherms for a 1,3,5-/1,2,4-/1,2,3-trichlorobenzene equimolar mixture in the modified $\mathbf{Fe_2(BDP)_3}$ structure at 433 K. Molecules that are able to reorient into a "face-to-face" configuration have higher saturation capacities.[300]

8. Conclusions and perspectives

The separation of hydrocarbon mixtures is a commercially important process. Adsorption has become an increasingly important process for separating hydrocarbon mixtures in the petrochemical industry since zeolite-based molecular sieves were commercialized in the middle of the past century. Microporous metal–organic frameworks have shown great application potential in hydrocarbon separation due to their adjustable pore dimensions, unique pore geometries, and functionalized pore surfaces. For example, the separation of valuable di-branched hexane isomers has now been accomplished by adsorption on MOFs. Additionally, it has been extensively demonstrated that the MIL series of metal–organic frameworks are very promising for the separation of xylene isomers. As well, the unprecedented discoveries of MOFs, such as **SIFSIX-1-Cu** and **NbOFFIVE-1-Ni**, for efficient acetylene/ethylene and propylene/propane separations are really encouraging.

The numerous choices of metal salts and the nearly infinite variability of organic linkers make it possible to design MOFs with desired pore structures and properties for task-specific adsorption applications. At present, more than 20 000 MOFs have been reported over the past decade. There is a seeming necessity for research interests over the coming decades to be heavily focused on adapting novel MOFs to industrial applications. For this purpose, using state-of-the-art molecular simulation methodologies allows for screening of large databases of real and predicted metal–organic framework structures, and might play an important role in partnership with experimental work in this field.

Due to the highly porous nature of MOFs, binder materials are often required to be blended with the MOF materials and thus to be packed into different forms of aggregated morphologies such as beads and pellets in order to provide adequate mechanical strength and to reduce the pressure drop across the adsorbent columns. The effects of such packing on the performance in hydrocarbon separation have been less well explored, but certainly need to be fully explored by such means as breakthrough experiments. It could be expected that the industrial usage of some promising MOFs will be implemented for hydrocarbon separation in the near future, as an increasing number of novel MOF materials are being discovered and evaluated.

Acknowledgements

This work was supported by an Award AX-1730 from the Welch Foundation (BC).

Notes and references

1 R. B. Eldridge, *Ind. Eng. Chem. Res.*, 1993, **32**, 2208–2212.
2 O. M. Yaghi, G. M. Li and H. L. Li, *Nature*, 1995, **378**, 703–706.
3 O. M. Yaghi and H. L. Li, *J. Am. Chem. Soc.*, 1995, **117**, 10401–10402.

4 B. L. Chen, M. Eddaoudi, S. T. Hyde, M. O'Keeffe and O. M. Yaghi, *Science*, 2001, **291**, 1021–1023.
5 J. L. C. Rowsell, E. C. Spencer, J. Eckert, J. A. K. Howard and O. M. Yaghi, *Science*, 2005, **309**, 1350–1354.
6 S. Kitagawa, R. Kitaura and S. Noro, *Angew. Chem., Int. Ed.*, 2004, **43**, 2334–2375.
7 S. Noro, R. Kitaura, M. Kondo, S. Kitagawa, T. Ishii, H. Matsuzaka and M. Yamashita, *J. Am. Chem. Soc.*, 2002, **124**, 2568–2583.
8 S. Q. Ma and H. C. Zhou, *J. Am. Chem. Soc.*, 2006, **128**, 11734–11735.
9 M. W. Zhang, Y. P. Chen and H. C. Zhou, *CrystEngComm*, 2013, **15**, 9544–9552.
10 J. L. C. Rowsell and O. M. Yaghi, *Microporous Mesoporous Mater.*, 2004, **73**, 3–14.
11 M. Eddaoudi, D. B. Moler, H. L. Li, B. L. Chen, T. M. Reineke, M. O'Keeffe and O. M. Yaghi, *Acc. Chem. Res.*, 2001, **34**, 319–330.
12 J. R. Long and O. M. Yaghi, *Chem. Soc. Rev.*, 2009, **38**, 1213–1214.
13 H. Furukawa, K. E. Cordova, M. O'Keeffe and O. M. Yaghi, *Science*, 2013, **341**, 1230444.
14 A. U. Czaja, N. Trukhan and U. Muller, *Chem. Soc. Rev.*, 2009, **38**, 1284–1293.
15 L. J. Murray, M. Dinca and J. R. Long, *Chem. Soc. Rev.*, 2009, **38**, 1294–1314.
16 Z. Q. Wang and S. M. Cohen, *Chem. Soc. Rev.*, 2009, **38**, 1315–1329.
17 J. R. Li, R. J. Kuppler and H. C. Zhou, *Chem. Soc. Rev.*, 2009, **38**, 1477–1504.
18 Z. R. Herm, E. D. Bloch and J. R. Long, *Chem. Mater.*, 2014, **26**, 323–338.
19 D. Banerjee, J. Liu and P. K. Thallapally, *Comments Inorg. Chem.*, 2015, **35**, 18–38.
20 J. R. Li, J. Sculley and H. C. Zhou, *Chem. Rev.*, 2012, **112**, 869–932.
21 H. H. Wu, Q. H. Gong, D. H. Olson and J. Li, *Chem. Rev.*, 2012, **112**, 836–868.
22 R. T. Yang, *Adsorbents: fundamentals and applications*, Wiley-Interscience, Hoboken, N.J., 2003.
23 R. T. Yang, *Gas separation by adsorption processes*, Butterworths, Boston, 1987.
24 F. A. Henglein, *Chemical technology*, Pergamon Press, Oxford, New York, 1st English edn, 1968.
25 H. Arakawa, M. Aresta, J. N. Armor, M. A. Barteau, E. J. Beckman, A. T. Bell, J. E. Bercaw, C. Creutz, E. Dinjus, D. A. Dixon, K. Domen, D. L. DuBois, J. Eckert, E. Fujita, D. H. Gibson, W. A. Goddard, D. W. Goodman, J. Keller, G. J. Kubas, H. H. Kung, J. E. Lyons, L. E. Manzer, T. J. Marks, K. Morokuma, K. M. Nicholas, R. Periana, L. Que, J. Rostrup-Nielson, W. M. H. Sachtler, L. D. Schmidt, A. Sen, G. A. Somorjai, P. C. Stair, B. R. Stults and W. Tumas, *Chem. Rev.*, 2001, **101**, 953–996.
26 X. G. Guo, G. Z. Fang, G. Li, H. Ma, H. J. Fan, L. Yu, C. Ma, X. Wu, D. H. Deng, M. M. Wei, D. L. Tan, R. Si, S. Zhang, J. Q. Li, L. T. Sun, Z. C. Tang, X. L. Pan and X. H. Bao, *Science*, 2014, **344**, 616–619.
27 S. D. Zhou, J. L. Li, X. N. Wu, M. Schlangen and H. Schwarz, *Angew. Chem., Int. Ed.*, 2016, **55**, 441–444.
28 J. W. Yoon, J. S. Lee, S. Lee, K. H. Cho, Y. K. Hwang, M. Daturi, C. H. Jun, R. Krishna and J. S. Chang, *Chem. – Eur. J.*, 2015, **21**, 18431–18438.
29 T. F. Xia, J. F. Cai, H. Z. Wang, X. Duan, Y. J. Cui, Y. Yang and G. D. Qian, *Microporous Mesoporous Mater.*, 2015, **215**, 109–115.
30 Y. X. Tan, Y. P. He and J. Zhang, *RSC Adv.*, 2015, **5**, 7794–7797.
31 K. Liu, D. X. Ma, B. Y. Li, Y. Li, K. X. Yao, Z. J. Zhang, Y. Han and Z. Shi, *J. Mater. Chem. A*, 2014, **2**, 15823–15828.
32 K. Liu, B. Y. Li, Y. Li, X. Li, F. Yang, G. Zeng, Y. Peng, Z. J. Zhang, G. H. Li, Z. Shi, S. H. Feng and D. T. Song, *Chem. Commun.*, 2014, **50**, 5031–5033.
33 Y. B. Huang, Z. J. Lin, H. R. Fu, F. Wang, M. Shen, X. S. Wang and R. Cao, *ChemSusChem*, 2014, **7**, 2647–2653.
34 Y. B. He, C. L. Song, Y. J. Ling, C. D. Wu, R. Krishna and B. L. Chen, *APL Mater.*, 2014, **2**, 124102.
35 X. Duan, Y. B. He, Y. J. Cui, Y. Yang, R. Krishna, B. L. Chen and G. D. Qian, *RSC Adv.*, 2014, **4**, 23058–23063.
36 H. Alawisi, B. Li, Y. B. He, H. D. Arman, A. M. Asiri, H. L. Wang and B. L. Chen, *Cryst. Growth Des.*, 2014, **14**, 2522–2526.
37 H. Xu, J. F. Cai, S. C. Xiang, Z. J. Zhang, C. D. Wu, X. T. Rao, Y. J. Cui, Y. Yang, R. Krishna, B. L. Chen and G. D. Qian, *J. Mater. Chem. A*, 2013, **1**, 9916–9921.
38 X. Duan, J. F. Cai, J. C. Yu, C. D. Wu, Y. J. Cui, Y. Yang and G. D. Qian, *Microporous Mesoporous Mater.*, 2013, **181**, 99–104.
39 G. H. Chen, Z. J. Zhang, S. C. Xiang and B. L. Chen, *CrystEngComm*, 2013, **15**, 5232–5235.
40 J. F. Cai, J. C. Yu, H. Xu, Y. B. He, X. Duan, Y. J. Cui, C. D. Wu, B. L. Chen and G. D. Qian, *Cryst. Growth Des.*, 2013, **13**, 2094–2097.
41 Z. J. Zhang, S. C. Xiang, K. L. Hong, M. C. Das, H. D. Arman, M. Garcia, J. U. Mondal, K. M. Thomas and B. L. Chen, *Inorg. Chem.*, 2012, **51**, 4947–4953.
42 Y. B. He, Z. J. Zhang, S. C. Xiang, F. R. Fronczek, R. Krishna and B. L. Chen, *Chem. – Eur. J.*, 2012, **18**, 613–619.
43 J. Li, H. R. Fu, J. Zhang, L. S. Zheng and J. Tao, *Inorg. Chem.*, 2015, **54**, 3093–3095.
44 X. Duan, Q. Zhang, J. F. Cai, Y. Yang, Y. J. Cui, Y. B. He, C. D. Wu, R. Krishna, B. Chen and G. D. Qian, *J. Mater. Chem. A*, 2014, **2**, 2628–2633.
45 X. Duan, Q. Zhang, J. F. Cai, Y. J. Cui, C. D. Wu, Y. Yang and G. D. Qian, *Microporous Mesoporous Mater.*, 2014, **190**, 32–37.
46 D. Yan, B. L. Chen and Q. Duan, *Inorg. Chem. Commun.*, 2014, **49**, 34–36.
47 J. F. Cai, H. Z. Wang, H. L. Wang, X. Duan, Z. Y. Wang, Y. J. Cui, Y. Yang, B. L. Chen and G. D. Qian, *RSC Adv.*, 2015, **5**, 77417–77422.
48 A. Schneemann, E. D. Bloch, S. Henke, P. L. Llewellyn, J. R. Long and R. A. Fischer, *Chem. – Eur. J.*, 2015, **21**, 18764–18769.

49 Y. He, Z. Zhang, S. Xiang, F. R. Fronczek, R. Krishna and B. Chen, *Chem. – Eur. J.*, 2012, **18**, 613–619.
50 Y. X. Tan, Y. Zhang, Y. P. He, Y. J. Zheng and J. Zhang, *Inorg. Chem.*, 2014, **53**, 12973–12976.
51 X. X. Zhang, P. Xiao, C. H. Zhan, B. Liu, R. Q. Zhong, L. Y. Yang, C. Y. Sun, H. Liu, Y. Pan, G. J. Chen and N. Li, *Ind. Eng. Chem. Res.*, 2015, **54**, 7890–7898.
52 M. C. Das, H. Xu, S. C. Xiang, Z. J. Zhang, H. D. Arman, G. D. Qian and B. L. Chen, *Chem. – Eur. J.*, 2011, **17**, 7817–7822.
53 S. Couck, E. Gobechiya, C. E. A. Kirschhock, P. Serra-Crespo, J. Juan-Alcaniz, A. M. Joaristi, E. Stavitski, J. Gascon, F. Kapteijn, G. V. Baron and J. F. M. Denayer, *ChemSusChem*, 2012, **5**, 740–750.
54 Y. B. He, Z. J. Zhang, S. C. Xiang, H. Wu, F. R. Fronczek, W. Zhou, R. Krishna, M. O'Keeffe and B. L. Chen, *Chem. – Eur. J.*, 2012, **18**, 1901–1904.
55 Y. S. Xue, Y. B. He, S. B. Ren, Y. F. Yue, L. Zhou, Y. Z. Li, H. B. Du, X. Z. You and B. L. Chen, *J. Mater. Chem.*, 2012, **22**, 10195–10199.
56 H. M. Wen, B. Li, H. L. Wang, C. D. Wu, K. Alfooty, R. Krishna and B. L. Chen, *Chem. Commun.*, 2015, **51**, 5610–5613.
57 R. Y. Zou, X. L. Ren, F. Huang, Y. F. Zhao, J. Liu, X. P. Jing, F. H. Liao, Y. X. Wang, J. H. Lin, R. D. Zou and J. L. Sun, *J. Mater. Chem. A*, 2015, **3**, 23493–23500.
58 Y. X. Hu, S. C. Xiang, W. W. Zhang, Z. X. Zhang, L. Wang, J. F. Bai and B. L. Chen, *Chem. Commun.*, 2009, 7551–7553.
59 Z. X. Chen, S. C. Xiang, H. D. Arman, P. Li, S. Tidrow, D. Y. Zhao and B. L. Chen, *Eur. J. Inorg. Chem.*, 2010, 3745–3749.
60 M. C. Das, H. Xu, Z. Wang, G. Srinivas, W. Zhou, Y.-F. Yue, V. N. Nesterov, G. Qian and B. Chen, *Chem. Commun.*, 2011, **47**, 11715–11717.
61 Z. Zhang, S. Xiang, Y.-S. Chen, S. Ma, Y. Lee, T. Phely-Bobin and B. Chen, *Inorg. Chem.*, 2010, **49**, 8444–8448.
62 S. Horike, Y. Inubushi, T. Hori, T. Fukushima and S. Kitagawa, *Chem. Sci.*, 2012, **3**, 116–120.
63 J. G. Duan, M. Higuchi, S. Horike, M. L. Foo, K. P. Rao, Y. Inubushi, T. Fukushima and S. Kitagawa, *Adv. Funct. Mater.*, 2013, **23**, 3525–3530.
64 S. Ma, D. Sun, X.-S. Wang and H.-C. Zhou, *Angew. Chem., Int. Ed.*, 2007, **46**, 2458–2462.
65 S. Ma, D. Sun, D. Yuan, X.-S. Wang and H.-C. Zhou, *J. Am. Chem. Soc.*, 2009, **131**, 6445–6451.
66 E. D. Bloch, W. L. Queen, R. Krishna, J. M. Zadrozny, C. M. Brown and J. R. Long, *Science*, 2012, **335**, 1606–1610.
67 Y. He, R. Krishna and B. Chen, *Energy Environ. Sci.*, 2012, **5**, 9107–9120.
68 A. M. Plonka, X. Y. Chen, H. Wang, R. Krishna, X. L. Dong, D. Banerjee, W. R. Woerner, Y. Han, J. Li and J. B. Parise, *Chem. Mater.*, 2016, **28**, 1636–1646.
69 R. K. Motkuri, H. V. R. Annapureddy, M. Vijaykumar, H. T. Schaef, P. F. Martin, B. P. McGrail, L. X. Dang, R. Krishna and P. K. Thallapally, *Nat. Commun.*, 2014, **5**, 4368.
70 S.-C. Xiang, Z. Zhang, C.-G. Zhao, K. Hong, X. Zhao, D.-R. Ding, M.-H. Xie, C.-D. Wu, M. C. Das, R. Gill, K. M. Thomas and B. Chen, *Nat. Commun.*, 2011, **2**, 204.
71 Y. He, Z. Zhang, S. Xiang, F. R. Fronczek, R. Krishna and B. Chen, *Chem. – Eur. J.*, 2012, **18**, 613–619.
72 T. L. Hu, H. L. Wang, B. Li, R. Krishna, H. Wu, W. Zhou, Y. F. Zhao, Y. Han, X. Wang, W. D. Zhu, Z. Z. Yao, S. C. Xiang and B. L. Chen, *Nat. Commun.*, 2015, **6**, 7328.
73 S. H. Yang, A. J. Ramirez-Cuesta, R. Newby, V. Garcia-Sakai, P. Manuel, S. K. Callear, S. I. Campbell, C. C. Tang and M. Schroder, *Nat. Chem.*, 2015, **7**, 121–129.
74 M. C. Das, Q. S. Guo, Y. B. He, J. Kim, C. G. Zhao, K. L. Hong, S. C. Xiang, Z. J. Zhang, K. M. Thomas, R. Krishna and B. L. Chen, *J. Am. Chem. Soc.*, 2012, **134**, 8703–8710.
75 Y. B. He, S. C. Xiang and B. L. Chen, *J. Am. Chem. Soc.*, 2011, **133**, 14570–14573.
76 X. L. Cui, K. J. Chen, H. B. Xing, Q. W. Yang, R. Krishna, Z. B. Bao, H. Wu, W. Zhou, X. L. Dong, Y. Han, B. Li, Q. L. Ren, M. J. Zaworotko and B. L. Chen, *Science*, 2016, **353**, 141–144.
77 Z. Bao, S. Alnemrat, L. Yu, I. Vasiliev, Q. Ren, X. Lu and S. Deng, *Langmuir*, 2011, **27**, 13554–13562.
78 J. Padin, S. U. Rege, R. T. Yang and L. S. Cheng, *Chem. Eng. Sci.*, 2000, **55**, 4525–4535.
79 F. A. Da Silva and A. E. Rodrigues, *Ind. Eng. Chem. Res.*, 1999, **38**, 2051–2057.
80 S. U. Rege, J. Padin and R. T. Yang, *AIChE J.*, 1998, **44**, 799–809.
81 M. Palomino, A. Cantin, A. Corma, S. Leiva, F. Rey and S. Valencia, *Chem. Commun.*, 2007, 1233–1235.
82 F. A. Da Silva and A. E. Rodrigues, *AIChE J.*, 2001, **47**, 341–357.
83 F. A. Da Silva and A. E. Rodrigues, *Ind. Eng. Chem. Res.*, 2001, **40**, 5758–5774.
84 A. Takahashi, R. T. Yang, C. L. Munson and D. Chinn, *Langmuir*, 2001, **17**, 8405–8413.
85 P. F. Bryan, *Sep. Purif. Rev.*, 2004, **33**, 157–182.
86 C. A. Grande and A. E. Rodrigues, *Ind. Eng. Chem. Res.*, 2004, **43**, 8057–8065.
87 F. Iucolano, P. Aprea, D. Caputo, C. Colella, M. Eic and Q. Huang, *Adsorption*, 2008, **14**, 241–246.
88 A. van Miltenburg, J. Gascon, W. Zhu, F. Kapteijn and J. A. Moulijn, *Adsorption*, 2008, **14**, 309–321.
89 G. Narin, V. F. D. Martins, M. Campo, A. M. Ribeiro, A. Ferreira, J. C. Santos, K. Schumann and A. E. Rodrigues, *Sep. Purif. Technol.*, 2014, **133**, 452–475.
90 D. Vargas-Hernandez, M. A. Perez-Cruz and R. Hernandez-Huesca, *Adsorption*, 2015, **21**, 153–163.
91 V. F. D. Martins, A. M. Ribeiro, M. G. Plaza, J. C. Santos, J. M. Loureiro, A. F. P. Ferreira and A. E. Rodrigues, *J. Chromatogr. A*, 2015, **1423**, 136–148.
92 M. C. Campo, M. C. Baptista, A. M. Ribeiro, A. Ferreira, J. C. Santos, C. Lutz, J. M. Loureiro and A. E. Rodrigues, *Adsorption*, 2014, **20**, 61–75.
93 M. C. Campo, A. M. Ribeiro, A. Ferreira, J. C. Santos, C. Lutz, J. M. Loureiro and A. E. Rodrigues, *Sep. Purif. Technol.*, 2013, **103**, 60–70.

94 Q. M. Wang, D. M. Shen, M. Bulow, M. L. Lau, S. G. Deng, F. R. Fitch, N. O. Lemcoff and J. Semanscin, *Microporous Mesoporous Mater.*, 2002, **55**, 217–230.
95 J. Ploegmakers, S. Japip and K. Nijmeijer, *J. Membr. Sci.*, 2013, **428**, 331–340.
96 T. M. Nicholson and S. K. Bhatia, *J. Phys. Chem. B*, 2006, **110**, 24834–24836.
97 T. M. Nicholson and S. K. Bhatia, *Adsorpt. Sci. Technol.*, 2007, **25**, 607–619.
98 S. Wang, Q. Yang and C. Zhong, *Sep. Purif. Technol.*, 2008, **60**, 30–35.
99 N. Lamia, M. Jorge, M. A. Granato, F. A. Almeida Paz, H. Chevreau and A. E. Rodrigues, *Chem. Eng. Sci.*, 2009, **64**, 3246–3259.
100 M. Jorge, N. Lamia and A. E. Rodrigues, *Colloids Surf., A*, 2010, **357**, 27–34.
101 M. Rubes, A. D. Wiersum, P. L. Llewellyn, L. Grajciar, O. Bludsky and P. Nachtigall, *J. Phys. Chem. C*, 2013, **117**, 11159–11167.
102 M. Fischer, J. R. B. Gomes, M. Froeba and M. Jorge, *Langmuir*, 2012, **28**, 8537–8549.
103 J. W. Yoon, I. T. Jang, K.-Y. Lee, Y. K. Hwang and J.-S. Chang, *Bull. Korean Chem. Soc.*, 2010, **31**, 220–223.
104 M. G. Plaza, A. M. Ribeiro, A. Ferreira, J. C. Santos, U. H. Lee, J.-S. Chang, J. M. Loureiro and A. E. Rodrigues, *Sep. Purif. Technol.*, 2012, **90**, 109–119.
105 V. F. D. Martins, A. M. Ribeiro, A. Ferreira, U. H. Lee, Y. K. Hwang, J. S. Chang, J. M. Loureiro and A. E. Rodrigues, *Sep. Purif. Technol.*, 2015, **149**, 445–456.
106 M. G. Plaza, A. F. P. Ferreira, J. C. Santos, A. M. Ribeiro, U. Mueller, N. Trukhan, J. M. Loureiro and A. E. Rodrigues, *Microporous Mesoporous Mater.*, 2012, **157**, 101–111.
107 A. F. P. Ferreira, J. C. Santos, M. G. Plaza, N. Lamia, J. M. Loureiro and A. E. Rodrigues, *Chem. Eng. J.*, 2011, **167**, 1–12.
108 M. Hartmann, S. Kunz, D. Himsl, O. Tangermann, S. Ernst and A. Wagener, *Langmuir*, 2008, **24**, 8634–8642.
109 M. Jorge, M. Fischer, J. R. B. Gomes, C. Siquet, J. C. Santos and A. E. Rodrigues, *Ind. Eng. Chem. Res.*, 2014, **53**, 15475–15487.
110 M. G. Plaza, A. M. Ribeiro, A. Ferreira, J. C. Santos, Y. K. Hwang, Y. K. Seo, U. H. Lee, J. S. Chang, J. M. Loureiro and A. E. Rodrigues, *Microporous Mesoporous Mater.*, 2012, **153**, 178–190.
111 J. W. Yoon, Y.-K. Seo, Y. K. Hwang, J.-S. Chang, H. Leclerc, S. Wuttke, P. Bazin, A. Vimont, M. Daturi, E. Bloch, P. L. Llewellyn, C. Serre, P. Horcajada, J.-M. Greneche, A. E. Rodrigues and G. Ferey, *Angew. Chem., Int. Ed.*, 2010, **49**, 5949–5952.
112 S. Wuttke, P. Bazin, A. Vimont, C. Serre, Y.-K. Seo, Y. K. Hwang, J.-S. Chang, G. Ferey and M. Daturi, *Chem. – Eur. J.*, 2012, **18**, 11959–11967.
113 H. Leclerc, A. Vimont, J.-C. Lavalley, M. Daturi, A. D. Wiersum, P. L. Llwellyn, P. Horcajada, G. Ferey and C. Serre, *Phys. Chem. Chem. Phys.*, 2011, **13**, 11748–11756.
114 S. J. Lee, J. W. Yoon, Y. K. Seo, M. B. Kim, S. K. Lee, U. H. Lee, Y. K. Hwang, Y. S. Bae and J. S. Chang, *Microporous Mesoporous Mater.*, 2014, **193**, 160–165.
115 X. F. Wu, Z. B. Bao, B. Yuan, J. Wang, Y. Q. Sun, H. M. Luo and S. G. Deng, *Microporous Mesoporous Mater.*, 2013, **180**, 114–122.
116 U. Bohme, B. Barth, C. Paula, A. Kuhnt, W. Schwieger, A. Mundstock, J. Caro and M. Hartmann, *Langmuir*, 2013, **29**, 8592–8600.
117 Y.-S. Bae, C. Y. Lee, K. C. Kim, O. K. Farha, P. Nickias, J. T. Hupp, S. T. Nguyen and R. Q. Snurr, *Angew. Chem., Int. Ed.*, 2012, **51**, 1857–1860.
118 D. L. Chen, H. Shang, W. D. Zhu and R. Krishna, *Chem. Eng. Sci.*, 2014, **117**, 407–415.
119 A. Mundstock, U. Bohme, B. Barth, M. Hartmann and J. Caro, *Chem. Ing. Tech.*, 2013, **85**, 1694–1699.
120 S. J. Geier, J. A. Mason, E. D. Bloch, W. L. Queen, M. R. Hudson, C. M. Brown and J. R. Long, *Chem. Sci.*, 2013, **4**, 2054–2061.
121 A. C. Kizzie, A. G. Wong-Foy and A. J. Matzger, *Langmuir*, 2011, **27**, 6368–6373.
122 J. B. DeCoste, G. W. Peterson, B. J. Schindler, K. L. Killops, M. A. Browe and J. J. Mahle, *J. Mater. Chem. A*, 2013, **1**, 11922–11932.
123 P. M. Schoenecker, C. G. Carson, H. Jasuja, C. J. J. Flemming and K. S. Walton, *Ind. Eng. Chem. Res.*, 2012, **51**, 6513–6519.
124 R. T. Yang and E. S. Kikkinides, *AIChE J.*, 1995, **41**, 509–517.
125 W. J. Jiang, Y. Yin, X. Q. Liu, X. Q. Yin, Y. Q. Shi and L. B. Sun, *J. Am. Chem. Soc.*, 2013, **135**, 8137–8140.
126 J. X. Qin, Z. M. Wang, X. Q. Liu, Y. X. Li and L. B. Sun, *J. Mater. Chem. A*, 2015, **3**, 12247–12251.
127 G. G. Chang, M. H. Huang, Y. Su, H. B. Xing, B. G. Su, Z. G. Zhang, Q. Q. Yang, Y. W. Yang, Q. L. Ren, Z. B. Bao and B. L. Chen, *Chem. Commun.*, 2015, **51**, 2859–2862.
128 B. Y. Li, Y. M. Zhang, R. Krishna, K. X. Yao, Y. Han, Z. L. Wu, D. X. Ma, Z. Shi, T. Pham, B. Space, J. Liu, P. K. Thallapally, J. Liu, M. Chrzanowski and S. Q. Ma, *J. Am. Chem. Soc.*, 2014, **136**, 8654–8660.
129 Y. M. Zhang, B. Y. Li, R. Krishna, Z. L. Wu, D. X. Ma, Z. Shi, T. Pham, K. Forrest, B. Space and S. Q. Ma, *Chem. Commun.*, 2015, **51**, 2714–2717.
130 G. G. Chang, Z. B. Bao, Q. L. Ren, S. G. Deng, Z. G. Zhang, B. G. Su, H. B. Xing and Y. W. Yang, *RSC Adv.*, 2014, **4**, 20230–20233.
131 S. Uchida, R. Kawamoto, H. Tagami, Y. Nakagawa and N. Mizuno, *J. Am. Chem. Soc.*, 2008, **130**, 12370–12376.
132 S. Uchida, R. Eguchi, S. Nakamura, Y. Ogasawara, N. Kurosawa and N. Mizuno, *Chem. Mater.*, 2012, **24**, 325–330.
133 P. Q. Liao, W. X. Zhang, J. P. Zhang and X. M. Chen, *Nat. Commun.*, 2015, **6**, 8697.
134 K. Li, D. H. Olson, J. Seidel, T. J. Emge, H. Gong, H. Zeng and J. Li, *J. Am. Chem. Soc.*, 2009, **131**, 10368–10369.
135 H. Bux, C. Chmelik, R. Krishna and J. Caro, *J. Membr. Sci.*, 2011, **369**, 284–289.
136 H. T. Kwon and H. K. Jeong, *Chem. Commun.*, 2013, **49**, 3854–3856.
137 M. Rungta, C. Zhang, W. J. Koros and L. R. Xu, *AIChE J.*, 2013, **59**, 3475–3489.

138 N. Hara, M. Yoshimune, H. Negishi, K. Haraya, S. Hara and T. Yamaguchi, *J. Jpn. Pet. Inst.*, 2015, **58**, 237–244.
139 H. T. Kwon, H. K. Jeong, A. S. Lee, H. S. An and J. S. Lee, *J. Am. Chem. Soc.*, 2015, **137**, 12304–12311.
140 Y. C. Pan, W. Liu, Y. J. Zhao, C. Q. Wang and Z. P. Lai, *J. Membr. Sci.*, 2015, **493**, 88–96.
141 Y. S. Lin, *Curr. Opin. Chem. Eng.*, 2015, **8**, 21–28.
142 V. M. A. Melgar, J. Kim and M. R. Othman, *J. Ind. Eng. Chem.*, 2015, **28**, 1–15.
143 S. L. Qiu, M. Xue and G. S. Zhu, *Chem. Soc. Rev.*, 2014, **43**, 6116–6140.
144 Z. Y. Yeo, S. P. Chai, P. W. Zhu and A. R. Mohamed, *RSC Adv.*, 2014, **4**, 54322–54334.
145 C. Chmelik, H. Bux, H. Voss and J. Caro, *Chem. Ing. Tech.*, 2011, **83**, 104–112.
146 K. Diaz, M. Lopez-Gonzalez, L. F. del Castillo and E. Riande, *J. Membr. Sci.*, 2011, **383**, 206–213.
147 C. Chmelik, D. Freude, H. Bux and J. Haase, *Microporous Mesoporous Mater.*, 2012, **147**, 135–141.
148 J. Kim, L. C. Lin, R. L. Martin, J. A. Swisher, M. Haranczyk and B. Smit, *Langmuir*, 2012, **28**, 11923–11928.
149 Y. Wu, H. Y. Chen, D. F. Liu, Y. Qian and H. X. Xi, *Chem. Eng. Sci.*, 2015, **124**, 144–153.
150 Y. C. Pan, T. Li, G. Lestari and Z. P. Lai, *J. Membr. Sci.*, 2012, **390**, 93–98.
151 D. F. Liu, X. L. Ma, H. X. Xi and Y. S. Lin, *J. Membr. Sci.*, 2014, **451**, 85–93.
152 S. Tanaka, T. Shimada, K. Fujita, Y. Miyake, K. Kida, K. Yogo, J. M. Denayer, M. Sugita and T. Takewaki, *J. Membr. Sci.*, 2014, **472**, 29–38.
153 C. Zhang, K. Zhang, L. R. Xu, Y. Labreche, B. Kraftschik and W. J. Koros, *AIChE J.*, 2014, **60**, 2625–2635.
154 N. Hara, M. Yoshimune, H. Negishi, K. Haraya, S. Hara and T. Yamaguchi, *Microporous Mesoporous Mater.*, 2015, **206**, 75–80.
155 H. T. Kwona and H. K. Jeong, *Chem. Eng. Sci.*, 2015, **124**, 20–26.
156 R. J. Verploegh, S. Nair and D. S. Sholl, *J. Am. Chem. Soc.*, 2015, **137**, 15760–15771.
157 J. Yu, Y. C. Pan, C. Q. Wang and Z. P. Lai, *Chem. Eng. Sci.*, 2016, **141**, 119–124.
158 H. T. Kwon and H. K. Jeong, *J. Am. Chem. Soc.*, 2013, **135**, 10763–10768.
159 C. Chmelik, *Microporous Mesoporous Mater.*, 2015, **216**, 138–145.
160 P. Krokidas, M. Castier, S. Moncho, E. Brothers and I. G. Economou, *J. Phys. Chem. C*, 2015, **119**, 27028–27037.
161 C. Zhang, R. P. Lively, K. Zhang, J. R. Johnson, O. Karvan and W. J. Koros, *J. Phys. Chem. Lett.*, 2012, **3**, 2130–2134.
162 C. Y. Lee, Y.-S. Bae, N. C. Jeong, O. K. Farha, A. A. Sarjeant, C. L. Stern, P. Nickias, R. Q. Snurr, J. T. Hupp and S. T. Nguyen, *J. Am. Chem. Soc.*, 2011, **133**, 5228–5231.
163 J. Pires, M. L. Pinto and V. K. Saini, *ACS Appl. Mater. Interfaces*, 2014, **6**, 12093–12099.
164 C. Gucuyener, J. van den Bergh, J. Gascon and F. Kapteijn, *J. Am. Chem. Soc.*, 2010, **132**, 17704–17706.
165 R. S. Pillai, M. L. Pinto, J. Pires, M. Jorge and J. R. B. Gomes, *ACS Appl. Mater. Interfaces*, 2015, **7**, 624–637.
166 J. van den Bergh, C. Gucuyener, E. A. Pidko, E. J. M. Hensen, J. Gascon and F. Kapteijn, *Chem. – Eur. J.*, 2011, **17**, 8832–8840.
167 D. L. Chen, N. W. Wang, C. H. Xu, G. M. Tu, W. D. Zhu and R. Krishna, *Microporous Mesoporous Mater.*, 2015, **208**, 55–65.
168 N. Nijem, H. Wu, P. Canepa, A. Marti, K. J. Balkus Jr., T. Thonhauser, J. Li and Y. J. Chabal, *J. Am. Chem. Soc.*, 2012, **134**, 15201–15204.
169 K. Kishida, Y. Watanabe, S. Horike, Y. Watanabe, Y. Okumura, Y. Hijikata, S. Sakaki and S. Kitagawa, *Eur. J. Inorg. Chem.*, 2014, 2747–2752.
170 K. Kishida, S. Horike, Y. Watanabe, M. Tahara, Y. Inubushi and S. Kitagawa, *Chem. – Asian J.*, 2014, **9**, 1643–1647.
171 T. Hähnel, G. Kalies, R. Krishna, J. Möllmer, J. Hofmann, M. Kobalz and H. Krautscheid, *Microporous Mesoporous Mater.*, 2016, **224**, 392–399.
172 L. B. Li, R. Krishna, Y. Wang, J. F. Yang, X. Q. Wang and J. P. Li, *J. Mater. Chem. A*, 2016, **4**, 751–755.
173 A. Cadiau, K. Adil, P. M. Bhatt, Y. Belmabkhout and M. Eddaoudi, *Science*, 2016, **353**, 137–140.
174 Z. R. Herm, B. M. Wiers, J. A. Mason, J. M. van Baten, M. R. Hudson, P. Zajdel, C. M. Brown, N. Masciocchi, R. Krishna and J. R. Long, *Science*, 2013, **340**, 960–964.
175 N. Chang, Z. Y. Gu and X. P. Yan, *J. Am. Chem. Soc.*, 2010, **132**, 13645–13647.
176 D. Peralta, G. Chaplais, A. Simon-Masseron, K. Barthelet and G. D. Pirngruber, *Ind. Eng. Chem. Res.*, 2012, **51**, 4692–4702.
177 B. L. Chen, C. D. Liang, J. Yang, D. S. Contreras, Y. L. Clancy, E. B. Lobkovsky, O. M. Yaghi and S. Dai, *Angew. Chem., Int. Ed.*, 2006, **45**, 1390–1393.
178 P. S. Barcia, D. Guimaraes, P. A. P. Mendes, J. A. C. Silva, V. Guillerm, H. Chevreau, C. Serre and A. E. Rodrigues, *Microporous Mesoporous Mater.*, 2011, **139**, 67–73.
179 Y. Ling, Z. X. Chen, F. P. Zhai, Y. M. Zhou, L. H. Weng and D. Y. Zhao, *Chem. Commun.*, 2011, **47**, 7197–7199.
180 Z. L. Fang, S. R. Zheng, J. B. Tan, S. L. Cai, J. Fan, X. Yan and W. G. Zhang, *J. Chromatogr. A*, 2013, **1285**, 132–138.
181 A. F. P. Ferreira, M. C. Mittelmeijer-Hazeleger, M. A. Granato, V. F. D. Martins, A. E. Rodrigues and G. Rothenberg, *Phys. Chem. Chem. Phys.*, 2013, **15**, 8795–8804.
182 P. A. P. Mendes, F. Ragon, A. E. Rodrigues, P. Horcajada, C. Serre and J. A. C. Silva, *Microporous Mesoporous Mater.*, 2013, **170**, 251–258.
183 T. Duerinck and J. F. M. Denayer, *Adsorption*, 2014, **20**, 251–259.
184 P. A. P. Mendes, P. Horcajada, S. Rives, H. Ren, A. E. Rodrigues, T. Devic, E. Magnier, P. Trens, H. Jobic, J. Ollivier, G. Maurin, C. Serre and J. A. C. Silva, *Adv. Funct. Mater.*, 2014, **24**, 7666–7673.
185 P. A. P. Mendes, A. E. Rodrigues, P. Horcajada, J. Eubank, T. Devic, C. Serre and J. A. C. Silva, *Adsorpt. Sci. Technol.*, 2014, **32**, 475–488.

186 P. A. P. Mendes, A. E. Rodrigues, P. Horcajada, C. Serre and J. A. C. Silva, *Microporous Mesoporous Mater.*, 2014, **194**, 146–156.
187 C. T. He, L. Jiang, Z. M. Ye, R. Krishna, Z. S. Zhong, P. Q. Liao, J. Q. Xu, G. F. Ouyang, J. P. Zhang and X. M. Chen, *J. Am. Chem. Soc.*, 2015, **137**, 7217–7223.
188 R. Krishna, *Phys. Chem. Chem. Phys.*, 2015, **17**, 39–59.
189 S. Couck, Y. Y. Liu, K. Leus, G. V. Baron, P. Van der Voort and J. P. M. Denayer, *Microporous Mesoporous Mater.*, 2015, **206**, 217–225.
190 S. Couck, T. Remy, G. V. Baron, J. Gascon, F. Kapteijn and J. F. M. Denayer, *Phys. Chem. Chem. Phys.*, 2010, **12**, 9413–9418.
191 V. Finsy, S. Calero, E. Garcia-Perez, P. J. Merkling, G. Vedts, D. E. De Vos, G. V. Baron and J. F. M. Denayer, *Phys. Chem. Chem. Phys.*, 2009, **11**, 3515–3521.
192 A. Zukal and M. Kubu, *Adsorption*, 2015, **21**, 99–105.
193 A. Zukal, M. Opanasenko, M. Rubes, P. Nachtigall and J. Jagiello, *Catal. Today*, 2015, **243**, 69–75.
194 L. Pan, D. H. Olson, L. R. Ciemnolonski, R. Heddy and J. Li, *Angew. Chem., Int. Ed.*, 2006, **45**, 616–619.
195 P. S. Barcia, F. Zapata, J. A. C. Silva, A. E. Rodrigues and B. Chen, *J. Phys. Chem. B*, 2007, **111**, 6101–6103.
196 D. Dubbeldam, C. J. Galvin, K. S. Walton, D. E. Ellis and R. Q. Snurr, *J. Am. Chem. Soc.*, 2008, **130**, 10884–10885.
197 N. A. Ramsahye, P. Trens, C. Shepherd, P. Gonzalez, T. K. Trung, F. Ragon and C. Serre, *Microporous Mesoporous Mater.*, 2014, **189**, 222–231.
198 D. Dubbeldam, R. Krishna, S. Calero and A. O. Yazaydin, *Angew. Chem., Int. Ed.*, 2012, **51**, 11867–11871.
199 M. Tu, S. Wannapaiboon, K. Khaletskaya and R. A. Fischer, *Adv. Funct. Mater.*, 2015, **25**, 4470–4479.
200 N. Chang, Z. Y. Gu, H. F. Wang and X. P. Yan, *Anal. Chem.*, 2011, **83**, 7094–7101.
201 S. Van der Perre, T. Van Assche, B. Bozbiyik, J. Lannoeye, D. E. De Vos, G. V. Baron and J. F. M. Denayer, *Langmuir*, 2014, **30**, 8416–8424.
202 L. Zhang, G. Qian, Z. J. Liu, Q. Cui, H. Y. Wang and H. Q. Yao, *Sep. Purif. Technol.*, 2015, **156**, 472–479.
203 M. T. Luebbers, T. Wu, L. Shen and R. I. Masel, *Langmuir*, 2010, **26**, 15625–15633.
204 A. H. Assen, Y. Belmabkhout, K. Adil, P. M. Bhatt, D. X. Xue, H. Jiang and M. Eddaoudi, *Angew. Chem., Int. Ed.*, 2015, **54**, 14353–14358.
205 Y. Wan, C. Chen, W. M. Xiao, L. J. Jian and N. Zhang, *Microporous Mesoporous Mater.*, 2013, **171**, 9–13.
206 S. Y. Nam and J. R. Dorgan, *J. Membr. Sci.*, 2007, **306**, 186–195.
207 L. D. Shiau and C. C. Yu, *Sep. Purif. Technol.*, 2009, **66**, 422–426.
208 S. B. Kuila and S. K. Ray, *Sep. Purif. Technol.*, 2014, **123**, 45–52.
209 A. S. Munich and F. O. R. L. Mertens, *CrystEngComm*, 2015, **17**, 438–447.
210 B. Manna, S. Mukherjee, A. V. Desai, S. Sharma, R. Krishna and S. K. Ghosh, *Chem. Commun.*, 2015, **51**, 15386–15389.
211 A. Karmakar, A. V. Desai, B. Manna, B. Joarder and S. K. Ghosh, *Chem. – Eur. J.*, 2015, **21**, 7071–7076.
212 C. X. Ren, L. X. Cai, C. Chen, B. Tan, Y. J. Zhang and J. Zhang, *J. Mater. Chem. A*, 2014, **2**, 9015–9019.
213 C. Yan, K. Li, S. C. Wei, H. P. Wang, L. Fu, M. Pan and C. Y. Su, *J. Mater. Chem.*, 2012, **22**, 9846–9852.
214 Y. X. Tan, Y. P. He and J. Zhang, *Inorg. Chem.*, 2012, **51**, 9649–9654.
215 Y. X. Tan, Y. P. He and J. Zhang, *ChemSusChem*, 2012, **5**, 1597–1601.
216 B. Joarder, A. K. Chaudhari and S. K. Ghosh, *Inorg. Chem.*, 2012, **51**, 4644–4649.
217 X. Q. Wang, J. Eckert, L. M. Liu and A. J. Jacobson, *Inorg. Chem.*, 2011, **50**, 2028–2036.
218 G. J. Ren, S. X. Liu, F. J. Ma, F. Wei, Q. Tang, Y. Yang, D. D. Liang, S. J. Li and Y. G. Chen, *J. Mater. Chem.*, 2011, **21**, 15909–15913.
219 F. J. Ma, S. X. Liu, D. D. Liang, G. J. Ren, F. Wei, Y. G. Chen and Z. M. Su, *J. Solid State Chem.*, 2011, **184**, 3034–3039.
220 Y. Hijikata, S. Horike, M. Sugimoto, H. Sato, R. Matsuda and S. Kitagawa, *Chem. – Eur. J.*, 2011, **17**, 5138–5144.
221 R. Yang, L. Li, Y. Xiong, J. R. Li, H. C. Zhou and C. Y. Su, *Chem. – Asian J.*, 2010, **5**, 2358–2368.
222 S. Galli, N. Masciocchi, V. Colombo, A. Maspero, G. Palmisano, F. J. Lopez-Garzon, M. Domingo-Garcia, I. Fernandez-Morales, E. Barea and J. A. R. Navarro, *Chem. Mater.*, 2010, **22**, 1664–1672.
223 L. Duan, Z. H. Wu, J. P. Ma, X. W. Wu and Y. B. Dong, *Inorg. Chem.*, 2010, **49**, 11164–11173.
224 J. B. Lin, J. P. Zhang, W. X. Zhang, W. Xue, D. X. Xue and X. M. Chen, *Inorg. Chem.*, 2009, **48**, 6652–6660.
225 G. Li, C. F. Zhu, X. B. Xi and Y. Cui, *Chem. Commun.*, 2009, 2118–2120, DOI: 10.1039/b901574d.
226 J. P. Zhang and X. M. Chen, *J. Am. Chem. Soc.*, 2008, **130**, 6010–6017.
227 S. Shimomura, S. Horike, R. Matsuda and S. Kitagawa, *J. Am. Chem. Soc.*, 2007, **129**, 10990–10991.
228 J. Y. Lee, D. H. Olson, L. Pan, T. J. Emge and J. Li, *Adv. Funct. Mater.*, 2007, **17**, 1255–1262.
229 S. Shimomura, R. Matsuda and S. Kitagawa, *Chem. Mater.*, 2010, **22**, 4129–4131.
230 E. Quartapelle Procopio, F. Linares, C. Montoro, V. Colombo, A. Maspero, E. Barea and J. A. R. Navarro, *Angew. Chem., Int. Ed.*, 2010, **49**, 7308–7311.
231 A. Karmakar, A. Kumar, A. K. Chaudhari, P. Samanta, A. V. Desai, R. Krishna and S. K. Ghosh, *Chem. – Eur. J.*, 2016, **22**, 4931–4937.
232 S. Mukherjee, B. Manna, A. V. Desai, Y. Yin, R. Krishna, R. Babarao and S. K. Ghosh, *Chem. Commun.*, 2016, **52**, 8215–8218.
233 M. A. Moreira, A. F. P. Ferreira, J. C. Santos, J. M. Loureiro and A. E. Rodrigues, *Chem. Eng. Technol.*, 2014, **37**, 1483–1492.
234 M. Minceva and A. E. Rodrigues, *AIChE J.*, 2007, **53**, 138–149.
235 R. R. Poissant, Y. N. Huang and R. A. Secco, *Microporous Mesoporous Mater.*, 2004, **74**, 231–238.

236 R. N. Devi, M. Edgar, J. Gonzalez, A. M. Z. Slawin, D. P. Tunstall, P. Grewal, P. A. Cox and P. A. Wright, *J. Phys. Chem. B*, 2004, **108**, 535–543.
237 L. Alaerts, C. E. A. Kirschhock, M. Maes, M. A. van der Veen, V. Finsy, A. Depla, J. A. Martens, G. V. Baron, P. A. Jacobs, J. E. M. Denayer and D. E. De Vos, *Angew. Chem., Int. Ed.*, 2007, **46**, 4293–4297.
238 V. Finsy, H. Verelst, L. Alaerts, D. De Vos, P. A. Jacobs, G. V. Baron and J. F. M. Denayer, *J. Am. Chem. Soc.*, 2008, **130**, 7110–7118.
239 T. Duerinck, S. Couck, F. Vermoortele, D. E. De Vos, G. V. Baron and J. F. M. Denayer, *Langmuir*, 2012, **28**, 13883–13891.
240 L. Alaerts, M. Maes, P. A. Jacobs, J. F. M. Denayer and D. E. De Vos, *Phys. Chem. Chem. Phys.*, 2008, **10**, 2979–2985.
241 A. Ghysels, M. Vandichel, T. Verstraelen, M. A. van der Veen, D. E. De Vos, M. Waroquier and V. Van Speybroeck, *Theor. Chem. Acc.*, 2012, **131**, 1234.
242 Z.-Y. Gu, D.-Q. Jiang, H.-F. Wang, X.-Y. Cui and X.-P. Yan, *J. Phys. Chem. C*, 2010, **114**, 311–316.
243 Z. Jin, H. Y. Zhao, X. J. Zhao, Q. R. Fang, J. R. Long and G. S. Zhu, *Chem. Commun.*, 2010, **46**, 8612–8614.
244 W. Huang, J. Jiang, D. Y. Wu, J. Xu, B. Xue and A. M. Kirillov, *Inorg. Chem.*, 2015, **54**, 10524–10526.
245 F. Vermoortele, M. Maes, P. Z. Moghadam, M. J. Lennox, F. Ragon, M. Boulhout, S. Biswas, K. G. M. Laurier, I. Beurroies, R. Denoyel, M. Roeffaers, N. Stock, T. Duren, C. Serre and D. E. De Vos, *J. Am. Chem. Soc.*, 2011, **133**, 18526–18529.
246 M. A. Moreira, J. C. Santos, A. F. P. Ferreira, J. M. Loureiro, F. Ragon, P. Horcajada, P. G. Yot, C. Serre and A. E. Rodrigues, *Microporous Mesoporous Mater.*, 2012, **158**, 229–234.
247 M. A. Moreira, J. C. Santos, A. F. P. Ferreira, J. M. Loureiro, F. Ragon, P. Horcajada, P. G. Yot, C. Serre and A. E. Rodrigues, *Langmuir*, 2012, **28**, 3494–3502.
248 A. Torres-Knoop, R. Krishna and D. Dubbeldam, *Angew. Chem., Int. Ed.*, 2014, **53**, 7774–7778.
249 J. E. Warren, C. G. Perkins, K. E. Jelfs, P. Boldrin, P. A. Chater, G. J. Miller, T. D. Manning, M. E. Briggs, K. C. Stylianou, J. B. Claridge and M. J. Rosseinsky, *Angew. Chem., Int. Ed.*, 2014, **53**, 4592–4596.
250 S. Mukherjee, B. Joarder, B. Manna, A. V. Desai, A. K. Chaudhari and S. K. Ghosh, *Sci. Rep.*, 2014, **4**, 5761.
251 R. Krishna, *RSC Adv.*, 2015, **5**, 52269–52295.
252 L. Alaerts, M. Maes, L. Giebeler, P. A. Jacobs, J. A. Martens, J. F. M. Denayer, C. E. A. Kirschhock and D. E. De Vos, *J. Am. Chem. Soc.*, 2008, **130**, 14170–14178.
253 V. Finsy, C. E. A. Kirschhock, G. Vedts, M. Maes, L. Alaerts, D. E. De Vos, G. V. Baron and J. F. M. Denayer, *Chem. – Eur. J.*, 2009, **15**, 7724–7731.
254 C. Lieder, S. Opelt, M. Dyballa, H. Henning, E. Klemm and M. Hunger, *J. Phys. Chem. C*, 2010, **114**, 16596–16602.
255 M. A. Moreira, J. C. Santos, A. F. P. Ferreira, J. M. Loureiro and A. E. Rodrigues, *Ind. Eng. Chem. Res.*, 2011, **50**, 7688–7695.
256 M. A. Moreira, J. C. Santos, A. F. P. Ferreira, U. Muller, N. Trukhan, J. M. Loureiro and A. E. Rodrigues, *Sep. Sci. Technol.*, 2011, **46**, 1995–2003.
257 T. Remy, G. V. Baron and J. F. M. Denayer, *Langmuir*, 2011, **27**, 13064–13071.
258 W. De Malsche, S. Van der Perre, S. Silverans, M. Maes, D. E. De Vos, F. Lynen and J. F. M. Denayer, *Microporous Mesoporous Mater.*, 2012, **162**, 1–5.
259 R. El Osta, A. Carlin-Sinclair, N. Guillou, R. I. Walton, F. Vermoortele, M. Maes, D. de Vos and F. Millange, *Chem. Mater.*, 2012, **24**, 2781–2791.
260 M. Maes, F. Vermoortele, M. Boulhout, T. Boudewijns, C. Kirschhock, R. Ameloot, I. Beurroies, R. Denoyel and D. E. De Vos, *Microporous Mesoporous Mater.*, 2012, **157**, 82–88.
261 C. X. Yang, S. S. Liu, H. F. Wang, S. W. Wang and X. P. Yan, *Analyst*, 2012, **137**, 133–139.
262 L. H. Duan, X. Y. Dong, Y. Y. Wu, H. L. Li, L. Wang and L. J. Song, *J. Porous Mater.*, 2013, **20**, 431–440.
263 D. I. Kolokolov, A. G. Stepanov and H. Jobic, *J. Phys. Chem. C*, 2014, **118**, 15978–15984.
264 Z. M. Yan, W. M. Zhang, J. Gao, Y. F. Lin, J. R. Li, Z. Lin and L. Zhang, *RSC Adv.*, 2015, **5**, 40094–40102.
265 H. Reinsch and D. De Vos, *Microporous Mesoporous Mater.*, 2014, **200**, 311–316.
266 G. H. Xu, X. G. Zhang, P. Guo, C. L. Pan, H. J. Zhang and C. Wang, *J. Am. Chem. Soc.*, 2010, **132**, 3656–3657.
267 F. Niekiel, J. Lannoeye, H. Reinsch, A. S. Munn, A. Heerwig, I. Zizak, S. Kaskel, R. I. Walton, D. de Vos, P. Llewellyn, A. Lieb, G. Maurin and N. Stock, *Inorg. Chem.*, 2014, **53**, 4610–4620.
268 M. Maes, F. Vermoortele, L. Alaerts, S. Couck, C. E. A. Kirschhock, J. F. M. Denayer and D. E. De Vos, *J. Am. Chem. Soc.*, 2010, **132**, 15277–15285.
269 S. Rives, H. Jobic, D. I. Kolokolov, A. A. Gabrienko, A. G. Stepanov, Y. Ke, B. Frick, T. Devic, G. Ferey and G. Maurin, *J. Phys. Chem. C*, 2013, **117**, 6293–6302.
270 S. Mukherjee, B. Joarder, A. V. Desai, B. Manna, R. Krishna and S. K. Ghosh, *Inorg. Chem.*, 2015, **54**, 4403–4408.
271 J. M. Castillo, T. J. H. Vlugt and S. Calero, *J. Phys. Chem. C*, 2009, **113**, 20869–20874.
272 N. Chang and X. P. Yan, *J. Chromatogr. A*, 2012, **1257**, 116–124.
273 M. A. Moreira, J. C. Santos, A. F. P. Ferreira, J. M. Loureiro, F. Ragon, P. Horcajada, K. E. Shim, Y. K. Hwang, U. H. Lee, J. S. Chang, C. Serre and A. E. Rodrigues, *Langmuir*, 2012, **28**, 5715–5723.
274 T. Duerinck, R. Bueno-Perez, F. Vermoortele, D. E. De Vos, S. Calero, G. V. Baron and J. F. M. Denayer, *J. Phys. Chem. C*, 2013, **117**, 12567–12578.
275 M. A. Granato, V. D. Martins, A. F. P. Ferreira and A. E. Rodrigues, *Microporous Mesoporous Mater.*, 2014, **190**, 165–170.
276 Z. M. Yan, J. N. Zheng, J. F. Chen, P. Tong, M. H. Lu, Z. Lin and L. Zhang, *J. Chromatogr. A*, 2014, **1366**, 45–53.
277 W. W. Zhao, C. Y. Zhang, Z. G. Yan, L. P. Bai, X. Y. Wang, H. L. Huang, Y. Y. Zhou, Y. B. Xie, F. S. Li and J. R. Li, *J. Chromatogr. A*, 2014, **1370**, 121–128.

278 X. Q. Zhang, Q. Han and M. Y. Ding, *RSC Adv.*, 2015, **5**, 1043–1050.
279 J. H. Cavka, S. Jakobsen, U. Olsbye, N. Guillou, C. Lamberti, S. Bordiga and K. P. Lillerud, *J. Am. Chem. Soc.*, 2008, **130**, 13850–13851.
280 J. M. Holcroft, K. J. Hartlieb, P. Z. Moghadam, J. G. Bell, G. Barin, D. P. Ferris, E. D. Bloch, M. M. Algaradah, M. S. Nassar, Y. Y. Botros, K. M. Thomas, J. R. Long, R. Q. Snurr and J. F. Stoddart, *J. Am. Chem. Soc.*, 2015, **137**, 5706–5719.
281 D. Peralta, G. Chaplais, A. Simon-Masseron, K. Barthelet, C. Chizallet, A.-A. Quoineaud and G. D. Pirngruber, *J. Am. Chem. Soc.*, 2012, **134**, 8115–8126.
282 D. Peralta, G. Chaplais, J. L. Paillaud, A. Simon-Masseron, K. Barthelet and G. D. Pirngruber, *Microporous Mesoporous Mater.*, 2013, **173**, 1–5.
283 M. Srivastava, P. K. Roy and A. Ramanan, *RSC Adv.*, 2016, **6**, 13426–13432.
284 K. Zhang, R. P. Lively, C. Zhang, R. R. Chance, W. J. Koros, D. S. Sholl and S. Nair, *J. Phys. Chem. Lett.*, 2013, **4**, 3618–3622.
285 P. S. Barcia, M. P. M. Nicolau, J. M. Gallegos, B. Chen, A. E. Rodrigues and J. A. C. Silva, *Microporous Mesoporous Mater.*, 2012, **155**, 220–226.
286 M. P. M. Nicolau, P. S. Barcia, J. M. Gallegos, J. A. C. Silva, A. E. Rodrigues and B. L. Chen, *J. Phys. Chem. C*, 2009, **113**, 13173–13179.
287 Kirk-Othmer, *Kirk-Othmer Encyclopedia of Chemical Technology*, John Wiley & Sons, Inc., New York, 2008.
288 B. Elvers, *Ullmann's Encyclopedia of Industrial Chemistry*, John Wiley & Sons, Inc., New York, 2006.
289 X.-Y. Cui, Z.-Y. Gu, D.-Q. Jiang, Y. Li, H.-F. Wang and X.-P. Yan, *Anal. Chem.*, 2009, **81**, 9771–9777.
290 R. Ahmad, A. G. Wong-Foy and A. J. Matzger, *Langmuir*, 2009, **25**, 11977–11979.
291 R. Ameloot, A. Liekens, L. Alaerts, M. Maes, A. Galarneau, B. Coq, G. Desmet, B. F. Sels, J. F. M. Denayer and D. E. De Vos, *Eur. J. Inorg. Chem.*, 2010, 3735–3738, DOI: 10.1002/ejic.201000494.
292 M. Maes, F. Vermoortele, L. Alaerts, J. F. M. Denayer and D. E. De Vos, *J. Phys. Chem. C*, 2011, **115**, 1051–1055.
293 C. X. Yang and X. P. Yan, *Anal. Chem.*, 2011, **83**, 7144–7150.
294 T. Remy, L. N. Ma, M. Maes, D. E. De Vos, G. V. Baron and J. F. M. Denayer, *Ind. Eng. Chem. Res.*, 2012, **51**, 14824–14833.
295 K. J. Hartlieb, J. M. Holcroft, P. Z. Moghadam, N. A. Vermeulen, M. M. Algaradah, M. S. Nassar, Y. Y. Botros, R. Q. Snurr and J. F. Stoddart, *J. Am. Chem. Soc.*, 2016, **138**, 2292–2301.
296 U. Beck and E. Löser, *Ullmann's Encyclopedia of Industrial Chemistry*, Wiley-VCH, Weinheim, 2011.
297 L. Alaerts, M. Maes, M. A. van der Veen, P. A. Jacobs and D. E. De Vos, *Phys. Chem. Chem. Phys.*, 2009, **11**, 2903–2911.
298 T. Bao, J. Zhang, W. P. Zhang and Z. L. Chen, *J. Chromatogr. A*, 2015, **1381**, 239–246.
299 V. Guillerm, F. Ragon, M. Dan-Hardi, T. Devic, M. Vishnuvarthan, B. Campo, A. Vimont, G. Clet, Q. Yang, G. Maurin, G. Ferey, A. Vittadini, S. Gross and C. Serre, *Angew. Chem., Int. Ed.*, 2012, **51**, 9267–9271.
300 A. Torres-Knoop, S. R. G. Balestra, R. Krishna, S. Calero and D. Dubbeldam, *ChemPhysChem*, 2015, **16**, 532–535.